Perspectives for predicting North Atlantic decadal sea surface temperature variability

Milan Klöwer
GEOMAR Helmholtz Centre for Ocean Research Kiel
Christian-Albrechts-Universität zu Kiel

Advisor: Prof. Dr. Mojib Latif
Co-advisor: Prof. Dr. Richard Greatbatch

A thesis submitted for the degree of

Bachelor of Science

in the subject

Physics of the Earth System: Meteorology, Oceanography and Geophysics

Kiel, July 2013

Abstract

The predictability of North Atlantic sea surface temperature (SST), that results from the delayed oceanic response to atmospheric forcing is investigated by means of a partial coupling experiment performed with the Kiel Climate Model. Observed North Atlantic Oscillation (NAO)-related heat flux anomalies from 1865 to 2000 force the model's ocean component to the climatic trajectory of the NAO but enable an otherwise free interaction between ocean and atmosphere. Hence, the model simulates a Meridional Overturning Circulation (MOC) that is consistent with the NAO and with observed SST. However, the simulated SST variability suffers from systematic errors. Statistical investigations with Canonical Correlation Analysis (CCA) identify a delayed link of 21 years between MOC and observed SST that corresponds to the Atlantic Multidecadal Oscillation (AMO). Using CCA as predictive tool leads to a prognosis of future changes in North Atlantic SST variability until 2021. Subsequently to the current positive phase of the AMO the results yield that North Atlantic SST is expected to cool after 2015.

Zusammenfassung

Die Vorhersagbarkeit von Meeresoberflächentemperaturen (SST), die aus der verzögerten ozeanischen Reaktion auf atmosphärischen Antrieb resultiert, wird im Nordatlantik mittels eines gekoppelten Experiments mit dem Kieler Klimamodell untersucht. Beobachtete, im Zusammenhang mit der Nordatlantischen Oszillation (NAO) stehenden, Wärmeflussanomalien von 1865 bis 2000 binden die Ozean-Komponente des Modells and die Klimatrajektorie der NAO aber erlauben gleichzeitig eine sonst freie Interaktion zwischen Ozean und Atmosphäre. Das Modell simuliert demnach eine meridionale Umwälzbewegung (MOC), die vereinbar mit den Beobachtungen von NAO Index und SST ist. Die simulierte SST hingegen beinhaltet systematische Fehler. Statistische Untersuchungen mittels Kanonischer Korrelationsanalyse (CCA) identifizieren einen verzögerten Zusammenhang von 21 Jahren zwischen MOC und beobachteter SST, der mit der Atlantischen Multidekaden Oszillation (AMO) übereinstimmt. CCA wird als Methode zur statistischen Vorhersage verwendet und ermöglicht so die Entwicklung der nordatlantischen SST bis 2021 zu prognostizieren. Auf die aktuelle Warmphase der AMO ist folglich eine Abkühlung der nordatlantischen SST ab 2015 zu erwarten.

Contents

Nomenclature

Roman Symbols

a	Coefficient of the AR(1)-Process
a_0, a_1	Coefficients of linear regression
$\vec{e}$	Eigenvector of the EOF analysis that refers to the spatial pattern
$\vec{F}$	Canonical correlation pattern
$\vec{f}$	Canonical eigenvector
$\mathbf{f}$	Matrix of eigenvectors $\vec{f}$
h	Sea bottom
m_X, m_Y	Dimensions of $\vec{X}, \vec{Y}$
$\vec{u}$	Velocity vector
v	Meridional velocity
$\vec{X}, \vec{Y}$	multivariate random variables
w	Vertical velocity
X, Y	univariate random variables
x_i, y_i	The ith realizations of X, Y
y	Latitude
y_t	Element of AR(1)-Process
z	Vertical coordinate referring to depth

Greek Symbols

α	Coefficient of the EOF analysis that refers to the PC
β	Canonical variable
$\frac{\partial}{\partial x}$	Partial derivative with respect to x
ϵ	Error
η	Explained variance
λ	Eigenvalue of the associated eigenvalue-problem
$\mu, \vec{\mu}$	Expected value
$\vec{\Psi}$	Vector of k_Y regarded PCs
ψ	Stream function
ρ	Correlation coefficient
$\Sigma_{\vec{X},\vec{Y}}$	Covariance matrix of $\vec{X}, \vec{Y}$
σ	Covariance of X, Y
$\hat{\Sigma}$	Sample covariance matrix
$\vec{\chi}$	Vector of k_X regarded PCs

Superscripts

$\bar{x}$	Mean of x
i, j, k	superscript indices
$\alpha^+, \vec{e}^+$	Re-normalized version of $\alpha, \vec{e}$
$\vec{X}'$	Anomalies of $\vec{X}$
T	Transposition of the assigned vector

Subscripts

t	declares the time-dependancy of the assigned variable
i, j, k	subscript indices

Other Symbols

$\mathrm{Cov}(\vec{X}, \vec{Y})$	Covariance matrix of $\vec{X}, \vec{Y}$
$\mathrm{Cov}(X, Y)$	Covariance of X, Y
$\mathcal{E}$	Expectation operator
$\mathcal{F}$	Matrix of canonical correlation patterns
$\langle \vec{a}, \vec{b} \rangle$	inner product (scalar product) of two vectors $\vec{a}, \vec{b}$
$\mathcal{SSE}$	Sum of squared errors
$\mathrm{Var}(X)$	Variance of X

Acronyms

AMOC	Atlantic Meridional Overturning Circulation
AR(1)	Autoregressive process of first order
CCA	Canonical Correlation Analysis
CDO	Climate Data Operators
ECHAM	Atmospheric general circulation model
ECMWF	European Center for Medium-Range Weather Forecasts, Reading, UK
EOF	Empirical Orthogonal Function
ERA	ECMWF Reanalysis Project
ERSST	Extended Reconstructed Sea Surface Temperature
GFDL	Geophysical Fluid Dynamics Laboratory
HadISST	Hadley Centre Global Sea Ice and Sea Surface Temperature
KCM	Kiel Climate Model
MOC	Meridional Overturning Circulation
NAC	North Atlantic Current
NADW	North Atlantic Deep Water

NAO	North Atlantic Oscillation
NCAR	National Center for Atmospheric Research
NCEP	National Center for Environmental Predicition
NEMO	Nucleus for European Modelling of the Ocean
NOAA	National Oceanic and Atmospheric Administration
LIM	Louvain-la-Neuve Ice Model
OASIS	Ocean atmosphere coupler
OPA	Océan Parallélisé ocean model
ORCA	Tripolar global ocean grid
PC	Principal Component
SST	Sea Surface Temperature
Sv	Sverdrup, 1 Sv = 10^6 m^3s^{-1}

Chapter 1

Introduction

One of the key regions of oceanic circulation is the North Atlantic due to its feature in forming North Atlantic Deep Water (NADW), a water mass that penetrates the world's oceans following the paths of the three-dimensional conveyor belt circulation [Broecker, 1991]. The picture of a few simplified streams connecting the ocean basins was critizied, but it still provides the idea of a global ocean circulation including flow at depth, where signals of local changes have the potential to propagate globally. Several efforts were carried out to divide the ocean circulation into components that are impacted by different sources of energy: the wind-driven circulation (mainly the upper few hundred meters) as well as the thermohaline circulation, that is supposed to result from changes in density due to cooling at high-latitudes. Nevertheless, it is still controversial were the energy comes from, that drives the ocean in regions which are not directly wind-affected [Wunsch, 2002]. Nowadays, the term *Meridional Overturning Circulation* (MOC) is widely used to refer to an oceanic circulation that includes the deep ocean, as there is an explicit definition: It is the meridional flow dependent on latitude and depth, that remains after zonally averaging [Stewart, 2008]. In the North Atlantic this involves features such as the gulf stream, its extension farther north: the North Atlantic Current (NAC), the sinking regions (Labrador Sea, Irminger Sea) that form NADW, as well as the southward return flow at depth (see Fig. 1.1). The amount of transported heat by the MOC is in the order of 1 PW ($=10^{15}$ W) [Hall & Bryden, 1982], hence changes of its strength have a large impact on the climate of the North Atlantic and its adjacent land areas [Pohlmann *et al.*, 2006] and presumably world wide. Understanding the physical processes that drive MOC variability is motivated due to the benefit that results if understanding leads to the ability of prediction. But, is there potential to predict changes in the MOC, or are they following a fully chaotic behaviour?

In the last decades many studies contributed to the understanding of spatial and temporal variations of the MOC. Bjerknes [1964]; Kushnir [1994] stated that the North Atlantic region

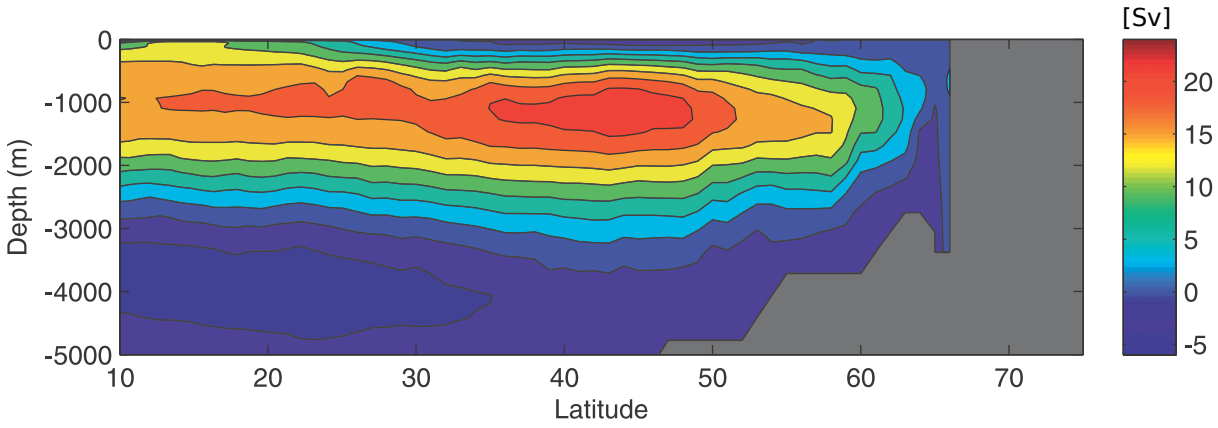

Figure 1.1: Mean Atlantic Meridional Overturning Circulation stream function [Sv]. The flow is parallel to isolines. Positive values indicate clockwise overturning yielding northward flow near the surface and southward flow at depth. From Grist *et al.* [2009], the stream function was calculated from a 100 year control run of GFDL2.1.

needs to be regarded as a coupled ocean-atmosphere system, in the sense that air and sea interact with each other through heat, momentum and freshwater fluxes. Additionally, it is suggested that the interactions are timescale-dependent: The atmosphere impacts the ocean on annual[1] time scales, whereas it is the ocean that influences the atmosphere on decadal time scales, in turn. In the North Atlantic, the dominant mode of atmospheric variability, that forces changes in the ocean is the North Atlantic Oscillation [Hurrell, 1995]. The NAO describes simultaneous variations of atmospheric pressure at high- and mid-latitudes (Fig. 1.2). The centers of action are located over Iceland and the Azores, hence, its index (Fig. 1.3) is a measurement for the strength of westwinds between 40°N and 60°N over the North Atlantic ocean and imprints many climatic parameters [Hurrell & Deser, 2010]. The NAO shows strongest variability on annual time scales as well as some power on the decadal band (Fig. 1.3). How do NAO and the MOC influence each other?

First, we have to note that NAO and MOC are spatially connected via the sea surface, hence every interaction between both will leave its imprint on the sea surface characteristics. Following the review paper of Latif *et al.* [2006b] there are at least two modes of oceanic variability that act on annual and longer time scales, one of them immediately related to the NAO, the other one heavily dependent on the MOC. Delworth & Greatbatch [2000]; Eden & Willebrand [2001] and Eden & Jung [2001] quantify that heat fluxes are the dominant atmospheric forcing to reproduce the oceanic variability on time scales of 60-70 years in models. In contrast, the momentum and

[1] Altough the terms *annual* and *decadal* are not concise, we use them in a sense that: *annual* refers to variations that are apparent while regarding annual mean values, but vanishing when an 11-year running mean is applied; *decadal* will be used for variability that is emphasized while regarding time series that are filtered with an 11-year running mean, hence *decadal* may cover periods up to a century as well.

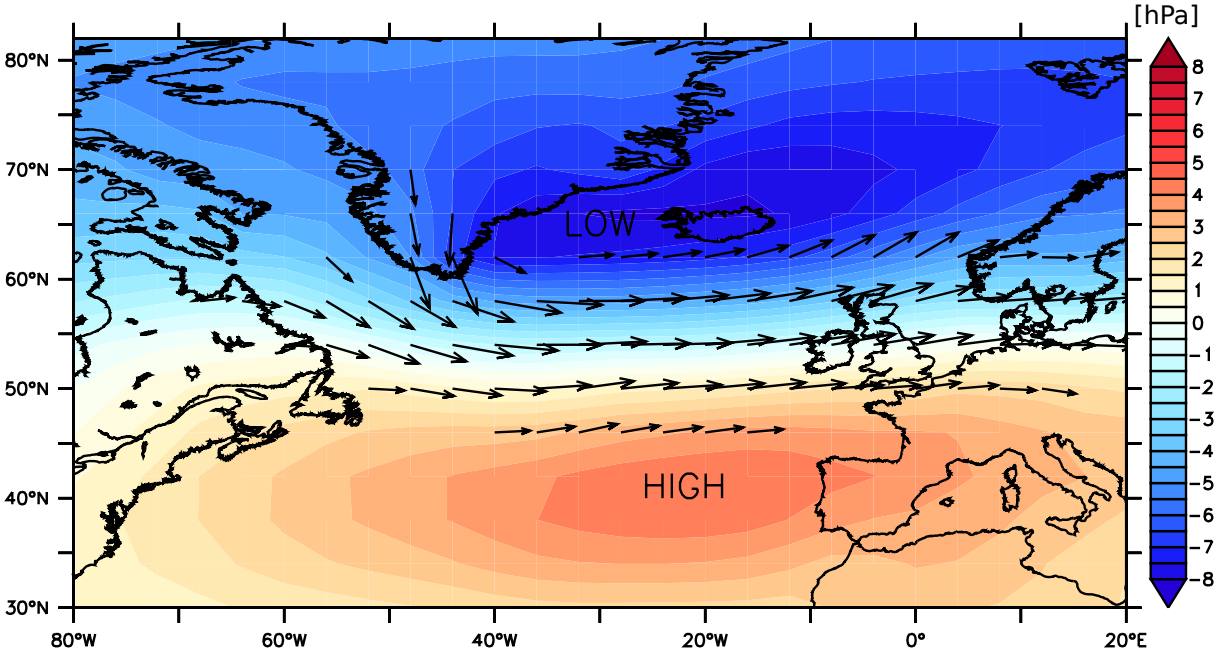

Figure 1.2: Spatial pattern of the North Atlantic Oscillation during winter. The positive phase of the NAO is associated with higher pressure over the Azores and lower pressure over Iceland yielding enhanced westwinds in the North Atlantic region. The geostrophic winds as follow from the strengthend pressure gradient are illustrated schematically. (The figure was calculated as first EOF from monthly ERA-Interim data, 1979-2012, December through March, over the illustrated region.)

freshwater fluxes are of minor importance. Since then, it is clear, that both modes leave their imprint on North Atlantic sea surface temperature (SST).

The former mode of oceanic variability, is known to be the immediate response of the sea surface due to NAO-related heat flux forcing. According to Eden & Jung [2001] there are three regions, where the NAO index explains most of the monthly heat flux anomalies: Labrador and Irminger Sea; the western mid-latitude North Atlantic and off the west coast of North Africa. Hence, this leads to a stationary three band pattern [Álvarez García *et al.*, 2008; Latif *et al.*, 2000a; Visbeck *et al.*, 1998] of SST anomalies mostly prevailing on annual time scales. Associated with this mode are positive (negative) SST anomalies in the Labrador and Irminger Sea during negative (positive) phases of the NAO.

The latter mode of oceanic variability, was identified by Schlesinger & Ramankutty [1994, 1995] as an oscillation of the North Atlantic SST, that varies basin-wide with a period of 50-70 years. Commonly used is the term *Atlantic Multidecadal Oscillation* (AMO, Kerr [2000]). In contrast to the annual mode described above, the AMO is explained by ocean dynamics [Eden & Greatbatch, 2003; Eden & Jung, 2001]. The signal of decadal changes in the NAO is simultaneously apparent in Labrador Sea Water thickness [Eden & Willebrand, 2001; Latif

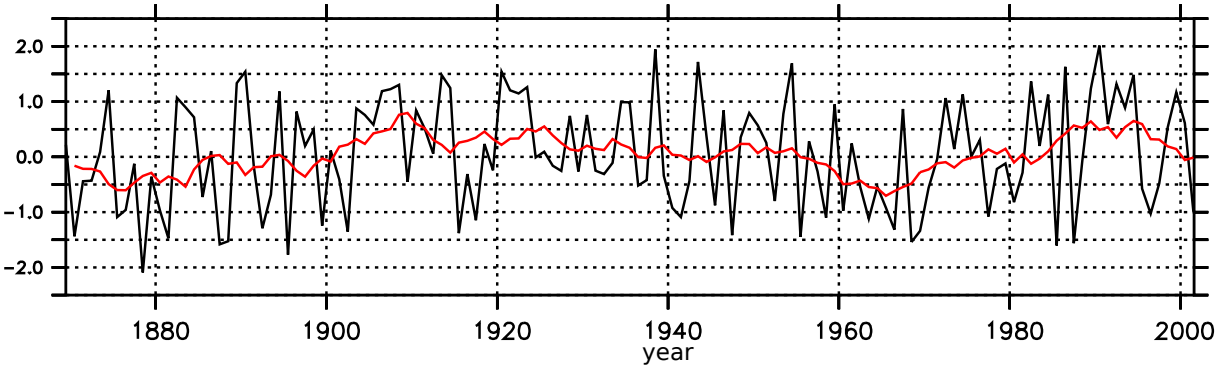

Figure 1.3: Station-based annual index of the North Atlantic Oscillation resulting from the difference in sea level pressure at Ponta Delgada, Azores and Stykkisholmur/Reykjavik, Iceland [Hurrell, 1995]. The red line indicates decadal changes as calculated by an 11-year running mean. The index is dimensionless through standardization.

et al., 2006a], a measure for the strength of deep water formation. Consequently, a stronger subpolar gyre circulation after 2-3 years and a stronger subtropical circulation after nearly a decade is induced [Eden & Willebrand, 2001]. A contributively strengthened MOC leads to enhanced oceanic heat transport [Eden & Greatbatch, 2003; Eden & Jung, 2001], which is reflected 10-20 years later in North Atlantic SST anomalies [Latif *et al.*, 2004]. There have been several discussions whether this mode is (i) a passive response of the ocean on atmospheric forced deep water formation; (ii) according to Bjerknes [1964] hypothesis a partial coupled mode, where the ocean integrates the annual atmospheric forcing and impacts the atmosphere on decadal time scales; or (iii) a fully coupled ocean-atmosphere covariability similar to those of the El-Niño Southern Oscillation phenomenon [Delworth & Greatbatch, 2000; Latif *et al.*, 2000a].

Some evidence has been provided that (i) is not the case as it is possible to reproduce decadal NAO variability, similiar to those observed, with an atmosphere-only model, driven with prescribed observed SST anomalies [Latif *et al.*, 2000a]. Hence, the ocean feeds back to the atmosphere at least on decadal time scales, supporting Bjerknes [1964] hypothesis. On the other hand, the NAO seems to be impacted not solely by the North Atlantic ocean, but is sensitive to changes in the Indian ocean and the Pacific region [Dima & Lohmann, 2007; Latif *et al.*, 2006b].

We recognize that the covariability of ocean and atmosphere in the North Atlantic is governed by an accumulation of climatic feedbacks (including momentum and freshwater fluxes, which is beyond the scope of this study), many of them poorly understood. Some of these feedbacks are, although physically reasonable, instantaneous reactions that do not provide any predictive skill. Looking for a potential for prediction it is necessary to focus on the ocean, as delayed feedbacks and slowly propagating signals [Getzlaff *et al.*, 2005] may lead to the application of a prognosis for the future [Sutton & Allen, 1997]. There is one mechanism, prevailing the

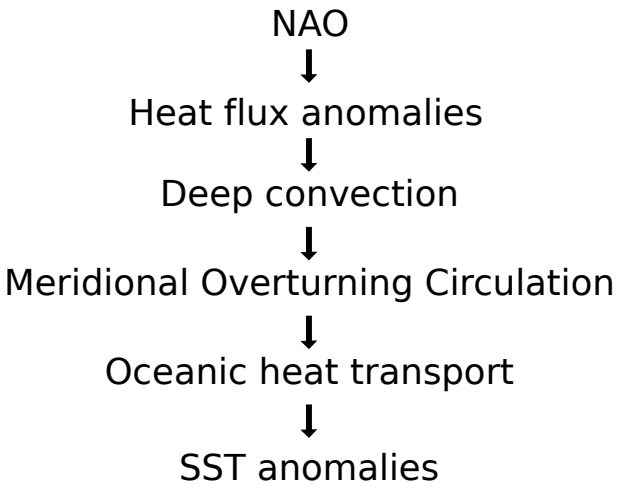

Figure 1.4: Schematic drawing of the predictive skill in the North Atlantic.

generation of SST anomalies on decadal time scales: Following the results that (i) NAO-related heat flux forcing leads to a consistent MOC [Eden & Jung, 2001] and (ii) the strength of the MOC determines North Atlantic decadal SST anomaly, Latif *et al.* [2006b] conclude that "the state of the multidecadal mode in the Atlantic may be predictable from the history of the NAO".

The objective of this study is to test whether the physical mechanism as drawn in Fig. 1.4 is statistically included in a coupled climate model and to perform a prediction of the future evolution of North Atlantic decadal SST variability based on statistical relationships between observations and model output. In order to attach the climate model to the climatic trajectory of the NAO during the twentieth century we follow the strategy of Eden & Jung [2001]. But, and this is in contrast to Eden & Jung [2001], we allow ocean and atmosphere to interact freely, since a coupled model is used.

The thesis is structured as follows: The data is presented in section 2.1 and a comprehensive introduction to the used methods are given in 2.2. Chapter 3 will discuss the models ability to reproduce SST variability which leads to the focus on simulated MOC in chapter 4. Having found a predictive skill we complete the present study with a prognosis of future North Atlantic SST evolution in chapter 5. In summary, the conclusions are drawn in chapter 6.

Chapter 2

Data and methodology

2.1 Data

We analyze sea surface temperatures (SST) and the Meridional Overturning Circulation (MOC) stream function from a partial coupling experiment of the Kiel Climate Model (KCM), which is described in section 2.1.1. In order to compare the experiment with observations we use two different SST reconstructions: NOAA' Extended Reconstructed Sea Surface Temperture (ERSST, section 2.1.2) and Hadley Centre Global Sea Ice and Sea Surface Temperature (HadISST, section 2.1.3).

2.1.1 Kiel Climate Model

A brief description of the KCM setting is following, further details are given in Park *et al.* [2009]. The KCM is a coupled climate model that consists of the ECHAM5[1] atmospheric model [Roeckner *et al.*, 2003] coupled via OASIS3 [Valcke, 2013] to the ocean and sea-ice model NEMO[2] [Madec, 2008]. NEMO contains the ocean general circulation model OPA9[3] and the sea-ice model LIM2[4]. ECHAM5 is a spectral model with a resolution of T31 ($3.75^\circ \times 3.75^\circ$) including 19 vertical levels for the atmosphere. The ocean model OPA9 is based on the tripolar ORCA2 grid, which provides a horizontal ocean resolution of 1.3° on average, with an equatorial refinement of 0.5°. The vertical is divided into 31 levels, including a free surface formulation and partial bottom cells. The tripolar ORCA2 grid divides the North Pole into two poles, one of them located in

[1] European Centre for Medium-Range Weather Forecasts (ECMWF) Hamburg atmospheric general circulation model version 5, developed at the Max Planck Institute for Meteorology (MPI), Hamburg

[2] Nucleus for European Modelling of the Ocean

[3] Océan Parallélisé version 9, developed at the Laboratory of Oceanography and Climatology (LOCEAN), Institut Pierre Simon Laplace (IPSL)

[4] Louvain-la-Neuve Ice Model version 2

North Canada, the other one in Siberia (Fig. Appendix .2). To exchange fields between ocean and atmosphere the OASIS3 coupler interpolates between the different grids that are used.

In general, the KCM is not using any form of flux correction or anomaly coupling, neither in heat fluxes, freshwater, nor in wind stress. However, the experiment analyzed here contains prescribed heat fluxes anomalies as explained in the next section.

Experimental design

The experimental setting implemented into the KCM is according to Eden & Jung [2001]. Heat flux anomalies from the NCEP-NCAR reanalysis [Kalnay *et al.*, 1996] were regressed onto the normalized monthly NAO index from 1958 to 2000 [Hurrell, 1995]. This leads to spatial regression patterns that are associated to the phase of the NAO. As the observed NAO Index is available from 1865 onwards it allows to reconstruct NAO-related heat fluxes since 1865. Thus, the forcing patterns were calculated by multiplying the NAO timeseries from 1865 to 2000 with the regression patterns yielding a term Q_{NAO} that is space and time dependent. Q_{NAO} is biggest in the regions where the NAO index explains most of the local heat fluxes (see Eden & Jung [2001], their Fig. 1(b)) and is added upon the simulated heat flux Q_{mod} yielding the total heat flux Q which is then felt by the model:

$$Q = Q_{mod} + Q_{NAO} \tag{2.1}$$

In general, as Q_{NAO} contains anomalies this term is small compared to Q_{mod}. This is especially the case for regions where the heat fluxes are not affected by the NAO: The term Q_{NAO} vanishes here. The experiment was performed five times resulting in five ensemble members, which differ in the stochastically perturbed initial conditions. In the following, we consider only the ensemble mean which is motivated as there is no particular interest in the chaotic behaviour of every member but in the oceanic response due to the forcing.

2.1.2 Extended Reconstructed Sea Surface Temperature

The Extended Reconstructed Sea Surface Temperature data set [Smith *et al.*, 2008] provides monthly 2° gridded SST from 1854 to present. The reconstruction was performed using statistical methods such as Empirical Orthogonal Function analysis to enlarge the sparsely available in situ data to a global set of SST data. The version used here is V3b, which does not contain satellite data to preserve a cold bias due to the availability of satellite records only during clear-sky conditions.

The analysis presented here is simultaneously performed with two data sets: ERSST and additionally the HadISST for comparison. We will primarily refer to the ERSST for clarity,

but in order to investigate the uncertainties that are included in the reconstructed SST we will present some aspects of the analysis of HadISST as well.

2.1.3 Hadley Centre Global Sea Ice and Sea Surface Temperature

The Hadley Centre Global Sea Ice and Sea Surface Temperature (HadISST) is a global data set of 1° gridded monthly SST. It is available since 1870 and is very similar to the ERSST data, but derived with different statistical methods. The similarity emphasizes the small uncertainties in both reconstructions, although we recognize that the uncertainties are considerable decreasing throughout the last half of the twentieth century [Smith *et al.*, 2008]. The version of HadISST used here is v1.1 and described in further detail in Rayner *et al.* [2003].

2.2 Methods

A short collection of some of the used statistical nomenclature is given in the Appendix. For clarification most of the methods are not presented in their empirical notation, which follows by substitution through the empirically estimated statistical moments: mean and (co-)variance. The methods explained here are given in further detail in Emery & Thomson [2001]; von Storch & Zwiers [1999]; Wilks [1995].

2.2.1 Data restriction

Prior to the present analysis we restrict the data temporally to the period of 1870-2000 and spatially to the region of the North Atlantic (100°W–10°E, 0°N–70°N). Additionally, we mask the following regions: Mediterranean sea, Hudson Bay, Pacific and partially the Labrador Sea. The spatial restriction is enlarged to 30°S for the MOC stream function.

All variables are considered as annual mean values and we regard only anomalies by subtracting the climatology that was calculated from 1870 to 2000 for every grid point, respectively. Furthermore, the data has been detrended as described in the next section.

2.2.2 Linear regression: detrending data

Linear regression is the approach of finding a model dependend on X that is able to represent Y upon an error ϵ. Regarding (x_i, y_i), for $i = \{1, ..., n\}$ as the realizations of X, Y. Then

$$y_i = a_0 + a_1 x_i + \epsilon_i \tag{2.2}$$

is the simple regression model with a_0, a_1 as unknown coefficients. The errors (or often called *residuals*) follow by rearranging equation 2.2

$$\epsilon_i = y_i - a_0 - a_1 x_i \tag{2.3}$$

To fit the regression model to Y we want to minimize the sum of the squared errors $\mathcal{SSE} = \sum_{i=1}^{n} \epsilon_i^2$. Therefore, the partial derivatives of $\mathcal{SSE}$ with respect to a_0, a_1

$$\sum_{i=1}^{n} (y_i - a_0 - a_1 x_i) = 0 \tag{2.4}$$

$$\sum_{i=1}^{n} (y_i - a_0 - a_1 x_i) x_i = 0 \tag{2.5}$$

are set to zero. With solutions

$$a_0 = \bar{y} - a_1 \bar{x} \tag{2.6}$$

$$a_1 = \frac{\sum_{i=1}^{n} x_i y_i - n\bar{x}\bar{y}}{\sum_{i=1}^{n} x_i^2 - n\bar{x}^2}. \tag{2.7}$$

where $\bar{x}, \bar{y}$ are the mean values. We regard Y as a function of time, with n time steps that correspond to the realizations y_i. X is then a vector containing x_i the n time steps in an increasing order. The trend is then defined as the slope a_1 of the linear regression. Hence, detrending a time series means subtracting the regression model

$$Y_{detr} = Y - (a_o + a_1 X). \tag{2.8}$$

Note that, detrending a time series eliminates the trend a_1 as well as the bias a_0. The model output data from KCM and both SST reconstructions have been detrended prior to the present analysis. This is motivated to preserve the correlations from being affected by trends and was applied on every grid point, respectively. Furthermore, it is not the objective of this study to analyze trends which are included in the SST reconstructions [Rayner *et al.*, 2003; Smith *et al.*, 2008] and in the MOC stream function (not shown). In case of the MOC the imprint of global climate change is not clear [Latif *et al.*, 2000b, 2006a]. However, trends in the MOC during the regarded period may result from variability on centennial and multi-centennial time scales [Menary *et al.*, 2012; Park & Latif, 2008, 2012].

2.2.3 Empirical Orthogonal Function

Empirical Orthogonal Function (EOF) analysis is the approach to expand a multivariate vector $\vec{X}$ into a finite series of empirically derived basis vectors $\vec{e}_i$ (which is actually the *Empirical Orthogonal Function*) and associated time-dependent coefficients α_i (*Principal Components*, PCs). This method was introduced to meteorology by Lorenz [1956] and described by Hotteling [1935] and Pearson [1902] in advance. First, we calculate anomalies of $\vec{X}$ by subtracting the expected value $\vec{\mu} = \mathcal{E}(\vec{X})$.

$$\vec{X}' = \vec{X} - \vec{\mu} \tag{2.9}$$

The finite series is then

$$\vec{X}' \approx \sum_{i=1}^{k} \alpha_i \vec{e}_i \tag{2.10}$$

Equality in 2.10 is in general only possible for $k \to m_X$, the dimension of $\vec{X}$. Indeed, in most cases the sum converges quickly to $\vec{X}'$, therefore it is possible to choose $k \ll m_X$. The PCs α_i are retained from projecting $\vec{e}_i$ onto $\vec{X}'$ via the inner product

$$\alpha_i = \langle \vec{X}', \vec{e}_i \rangle \tag{2.11}$$

The EOFs $\vec{e}_i$ are chosen to be orthogonal and accounting for a maximum of variation in $\vec{X}'$. The first EOF $\vec{e}_1$ is therefore found so that the error ϵ_1

$$\epsilon_1 = \mathcal{E}\left(\| \vec{X}' - \langle \vec{X}', \vec{e}_1 \rangle \vec{e}_1 \|^2 \right) \tag{2.12}$$

of reconstructing $\vec{X}'$ is minimized. $\| \cdot \|$ is the norm of a vector. Equation 2.12 is solved with Langrangian multipliers and given in von Storch & Zwiers [1999]. Minimizing the error ϵ_1 is the same as maximizing the variance of $\vec{e}_1$ that explains variations of $\vec{X}'$. The Lagrangian multiplier λ_i is the eigenvalue of the eigenvector $\vec{e}_i$, which is representing a proportion of the total variance. Hence, the explained variance η_k of the kth EOF is

$$\eta_k = \frac{\lambda_k}{\sum_i \lambda_i} \tag{2.13}$$

If the first EOF is calculated, the second EOF can be found with equation 2.12 by replacing $\vec{X}'$ with the vector $\vec{X}' - \langle \vec{X}', \vec{e}_1 \rangle \vec{e}_1$ that contains the variations of $\vec{X}'$ that can not be explained by the first EOF. This procedure is repeated analogously to obtain further EOFs.

In a physical sense, applying EOF analysis onto data that contains a spatial field of variables, each with a large sample of time steps, leads to patterns that are representing the dominant modes

of variability. Hence, the EOFs $\vec{e_i}$ are the spatial patterns and the PCs α_i their corresponding time series. In the case of equation 2.12 the patterns are dimensionless and the unit of $\vec{X}$ is carried by the time series. We replace the coefficients α_i and the eigenvectors $\vec{e_i}$ by their re-normalized versions indicated by + as superscript

$$\alpha_i^+ = \frac{1}{\sqrt{\lambda_i}}\alpha_i \quad , \quad \vec{e_i}^+ = \sqrt{\lambda_i}\vec{e_i} \tag{2.14}$$

so that

$$\mathrm{Var}(\alpha_i^+) = 1. \tag{2.15}$$

Hence, the time series is now dimensionless. Instead, the patterns $\vec{e_i}$ have now the unit of $\vec{X}$. For the present analysis the EOF analysis was applied on detrended data as described in section 2.2.2.

2.2.4 Canonical Correlation Analysis

The classical correlation as defined by Pearson is designed to study the linear relation between two univariate variables X, Y. The Canonical Correlation Analysis (CCA) was introduced by Hotteling [1936] and allows to study the linear relation of two *multi*variate variables $\vec{X}$ and $\vec{Y}$. Let m_X, m_Y be the dimensions of $\vec{X}, \vec{Y}$, respectively. First, considering linear combinations β_X, β_Y of $\vec{X}, \vec{Y}$ by calculating the inner products of $\vec{X}, \vec{Y}$ with vectors $\vec{f}_X, \vec{f}_Y$ of same dimensions m_X, m_Y.

$$\beta_X = \langle \vec{X}, \vec{f}_X \rangle \quad , \quad \beta_Y = \langle \vec{Y}, \vec{f}_Y \rangle \tag{2.16}$$

β_X, β_Y are called *canonical variables*. The objective of CCA is now that the correlation of the canonical variables

$$\rho = \frac{Cov(\beta^X, \beta^Y)}{\sqrt{Var(\beta^X)Var(\beta^Y)}} \tag{2.17}$$

is maximized. The solution of equation 2.17 is derived with Langrangian mulitpliers and given in von Storch & Zwiers [1999]. This leads to an eigenvalue-problem of the eigenvectors $\vec{f}_X, \vec{f}_Y$. The associated eigenvalue λ is related to the correlation ρ that we wanted to maximize by $\rho = \sqrt{\lambda}$. Therefore, choosing the largest eigenvalue λ_1 leads to the first pair of eigenvectors $\vec{f}_X^1, \vec{f}_Y^1$ and the associated first pair of canonical variables β_X^1, β_Y^1. More pairs of canonical variables are found by chosing next smaller eigenvalues $\lambda_{i+1} < \lambda_i$. Having found the canonical variables β_X^i, β_Y^i for $i = \{1, ..., m\}$, whereas m is the minimum of $\{m_X, m_Y\}$ we arrange them in vectors

$$\vec{\beta_X} = \{\beta_X^1, ..., \beta_X^m\} \quad , \quad \vec{\beta_Y} = \{\beta_Y^1, ..., \beta_Y^m\}. \tag{2.18}$$

Similarly, we arrange the eigenvectors $\vec{f}_X^i, \vec{f}_Y^i$ in $m \times m$ matrices $\mathbf{f}_X, \mathbf{f}_Y$ with the ith eigenvector in the ith column. Following von Storch & Zwiers [1999], it is now possible to obtain $\vec{X}, \vec{Y}$ through

$$\vec{X} = \mathcal{F}_X \vec{\beta_X} \quad , \quad \vec{Y} = \mathcal{F}_Y \vec{\beta_Y} \tag{2.19}$$

with matrices $\mathcal{F}_X, \mathcal{F}_Y$ that are derived as follows

$$\mathcal{F}_X = \Sigma_{\vec{X},\vec{X}} \mathbf{f}_X \quad , \quad \mathcal{F}_Y = \Sigma_{\vec{Y},\vec{Y}} \mathbf{f}_Y \tag{2.20}$$

where $\Sigma_{\vec{X},\vec{X}}$ is the covariance matrix of $\vec{X}$. The *canonical correlation patterns* $\vec{F}_X^i, \vec{F}_Y^i$ are contained in the columns of $\mathcal{F}_X, \mathcal{F}_Y$ and can be used to expand $\vec{X}, \vec{Y}$ into a finite series with $\vec{F}_X^i, \vec{F}_Y^i$ as basis vectors. Hence, we are now able to reconstruct $\vec{X}, \vec{Y}$ by

$$\vec{X} = \sum_i \beta_X^i \vec{F}_X^i \quad , \quad \vec{Y} = \sum_i \beta_Y^i \vec{F}_Y^i \tag{2.21}$$

2.2.5 CCA in EOF space

Canonical correlation analysis is applied in the EOF space, instead of the normal coordinate space (see e.g. Barnett & Preisendorfer [1987]; Eden & Willebrand [2001]; Latif *et al.* [2000a]) Using the re-normalized versions α_i^+ and $\vec{e_i}^+$ (see equation 2.14) CCA is then applied on the vectors $\vec{\chi}, \vec{\Psi}$

$$\vec{\chi} = \left(\alpha_1^{X+}, ..., \alpha_{k_X}^{X+}\right) \quad , \quad \vec{\Psi} = \left(\alpha_1^{Y+}, ..., \alpha_{k_Y}^{Y+}\right) \tag{2.22}$$

which contains the number of k_X, k_Y regarded PCs from the EOF analysis of $\vec{X}', \vec{Y}'$ (the anomalies of $\vec{X}, \vec{Y}$). This comes along with several advantages. First, the algebra of the eigenvalue-problem is simplified since the coefficients α_i are uncorrelated as follows from the orthogonality of the eigenvectors $\vec{e_i}$. Therefore, $\Sigma_{\vec{\chi},\vec{\chi}}$ and $\Sigma_{\vec{\Psi},\vec{\Psi}}$ are both identity matrices. Additionally, it is possible to choose the number of considered EOFs k_X, k_Y. We set $k_X = k_Y = 5$ to represent a large proportion of explained variance (approx. 60–70%, see Fig. 3.1) of the original field. Simultaneously, we are able to eliminate small scale variabilities by disregarding the high order EOFs.

As the original field has been transformed into EOF space in advance, it is necessary to reverse the transformation of equation 2.10 to obtain the canonical correlation patterns $\vec{F}_X^i, \vec{F}_Y^i$ in normal coordinate space by

$$\vec{F}_X^i = \sum_{j=1}^{k_X} \left(\vec{f_\chi}^{\,i}\right)_j \vec{e_X}^{j+} \quad , \quad \vec{F}_Y^i = \sum_{j=1}^{k_Y} \left(\vec{f_\Psi}^{\,i}\right)_j \vec{e_X}^{j+}. \tag{2.23}$$

where $(\cdot)_j$ denotes the jth element of $\vec{f^i}$. Note that the EOFs are used in their normalized version (see eq. 2.14), so that $\vec{e}$ carries the unit of the original field. We reconstruct the original field as described in equation 2.21. The canonical variables β_X, β_Y are then a linear combination of the k_X, k_Y regarded PCs and $\vec{F}_X^i, \vec{F}_Y^i$ refers to a linear combination of the spatial EOF patterns, as shown in equation 2.23.

2.2.6 Explained variance

The amount of variance η of $\vec{X}$ that can be explained by $\vec{Y}$ is

$$\eta = \frac{\mathrm{Var}(\vec{X}) - \mathrm{Var}(\vec{X} - \vec{Y})}{\mathrm{Var}(\vec{X})}. \tag{2.24}$$

Here $\vec{X}$ is the original field that we want to reconstruct with $\vec{Y}$. Note that, in the case of EOF (CCA) $\vec{Y}$ refers to the kth EOF (CCA) eigenmode as described in equation 2.10 (equation 2.21).

For the classical correlation between two univariate variables the calculation of explained variance is simplified. η is here defined as the squared correlation ρ^2.

2.2.7 Significance and simulation of random processes

We recognize that CCA is a technique that is to some degree always able to find eigenvectors $\vec{f_X}, \vec{f_Y}$ to correlate the canonical variables β_X, β_Y. Hence, it is necessary to investigate confidence levels for CCA to clearify whether the correlation ρ is significantly larger than the correlation that results from a random process with same degrees of freedom. Applying CCA in EOF space we consider two vectors $\vec{\chi}, \vec{\Psi}$ that contain the first $k_X = k_Y = 5$ PCs of the EOF analysis. Given a length of 131 years (1870-2000), or subsequently less while considering the application of a lag, determines the degrees of freedom. Thus, the null hypothesis is phrased by: The leading 5 PCs represent independent realizations of random process noise.

The elements of random vectors for $\vec{\chi}, \vec{\Psi}$ are simulated with a first order autoregressive model, which is called AR(1)-Process, as the next value y_t of the process is dependent on the previous one y_{t-1}. In general, AR(1)-Process is defined as

$$y_t = a y_{t-1} + \epsilon_t. \tag{2.25}$$

The coefficient a results from the autocorrelation function for lag = 1 of each PC. The error ϵ_t is normally distributed with unit variance.

We are now able to estimate the probability density distribution of the canonical correlation ρ from a number of $n = 10000$ random processes. We proceed in calculating the 95th- and

the 99th-percentile whose values are then taken as threshold to estimate whether the canonical correlation is significant or not.

Note that for the classical correlation significance levels can be derived from Student's t-distribution. In this study, for timeseries spanning 131 years (111 years while regarding a lag of 20 years) the threshold whether a correlation is significant at the 99%-level is 0.25 (0.24).

2.2.8 Stream function

A stream function is a scalar field that describes velocities defined in a vector field. The velocity needs to satisfy the two dimensional continuity equation

$$\nabla \cdot \vec{u} = \frac{\partial v}{\partial y} + \frac{\partial w}{\partial z} = 0 \tag{2.26}$$

which is here given on y-z-coordinates (y: Latitude, z: Depth). The velocity vector $\vec{u} = (v, w)$ contains the meridional velocity v and the vertical velocity w. The stream function ψ is then defined by

$$v = -\frac{\partial \psi}{\partial z} \quad , \quad w = \frac{\partial \psi}{\partial y} \tag{2.27}$$

(see Olbers *et al.* [2012]). Given the meridional velocity v as model ouput, we can average v zonally in the North Atlantic with the boundary conditions that there is no flow through the western or eastern boundary. $\vec{u}$ then satisfies the continuity equation 2.26. Integrating $v = \frac{\partial \psi}{\partial z}$ from bottom ($z = h$) to top ($z = 0$) with boundary conditions

$$\psi|_{z=h} = 0 \quad , \quad \psi|_{z=0} = 0 \tag{2.28}$$

yields the stream function on y-z-coordinates that represents the Atlantic Meridional Overturning Circulation.

In the case of the Kiel Climate Model, the stream function is calculated on the tripolar ORCA2 grid. Therefore, zonal averaging was applied on grid cells (where the laws of conservation are valid) with the same meridional index, which do not represent the same latitude (see Fig. Appendix.2). We chose the latitudes of zonal index 130, which lays approximately at 25°W to reassign the stream function with latitudes.

Chapter 3

Comparison of observed and simulated SST variability

This chapter presents the results of the respective analyses of variability patterns in space and time of the SST simulated by KCM as well as of the SST reconstructions ERSST and HadISST. Both SST reconstructions are considered to provide information about the their uncertainties.

3.1 Spatial patterns - EOF modes

The dominant modes of SST variability in the North Atlantic (0°N-70°N) are investigated by applying an EOF analysis from 1870 to 2000 as described in section 2.2.3. The explained variance of the respective EOF modes is shown in Fig. 3.1(a). The first EOF mode (hereafter EOF1, higher orders analogously) of ERSST and HadISST accounts for approximately 33% of the total variance (derived by equation 2.13). This most energetic mode represents basinwide SST variability of the same sign in ERSST and HadISST (Fig. 3.2(a)) and varies strongly on multi-decadal time scales as shown by the associated PC1 (Fig. 3.3(a)). Indeed, the time series of this mode is, with a correlation coefficient of 0.97 in ERSST and HadISST, nearly identical to the index of the Atlantic Multidecadal Oscillation (Schlesinger & Ramankutty [1994, 1995], defined as mean North Atlantic SST at 0°–60°N, Fig. 3.5).

In contrast, the dominant mode of SST variability EOF1 in the KCM ensemble mean accounts only for 24.6% of the total variance and represents a three band pattern as shown in Fig. 3.2(c). This pattern is known to result directly from the circulation anomalies of the lower atmosphere associated to the phase of the NAO [Latif *et al.*, 2000a; Visbeck *et al.*, 1998]: Anomalously high pressure over the Azores and low pressure over Iceland enhance the trade and west winds which impact the mixed-layer temperature through anomalous heat fluxes [Eden & Jung, 2001]. The

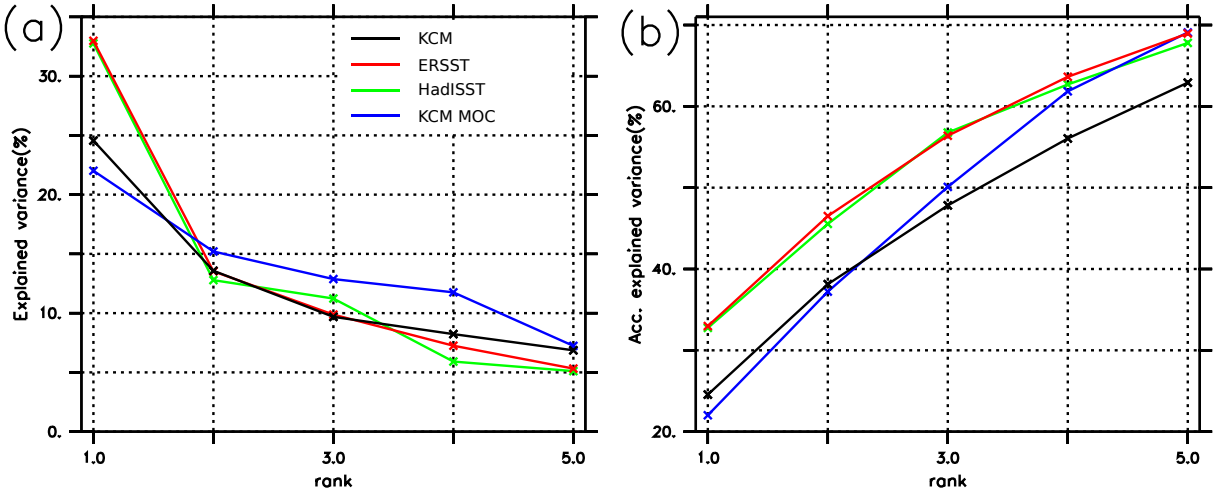

Figure 3.1: Eigenvalue spectrum of EOF analysis applied on detrended annual anomalies of North Atlantic SST (0°N–70°N, 1870-2000) of ERSST, HadISST, KCM Ensemble mean SST and of KCM ensemble mean MOC stream function (30°S–70°N, 1870-2000). (a) Explained variance [%], (b) accumulated explained variance [%].

relation between this mode of SST variability and the NAO is verified by a correlation coefficient of 0.56 on annual time scales and 0.81 on decadal time scales (11-year running mean is applied) calculated from PC1 (Fig. 3.3(a), black line) and the station-based annual NAO index (Fig. 1.3, Hurrell [1995]). Both correlations are significant at the 99%-level.

Although the three band pattern is dominant in KCM (Fig. 3.2(c)), this does not hold for ERSST and HadISST, where this pattern as shown in Fig. 3.2(b) accounts for the second most energetic mode EOF2, explaining 13.5% of the total variance. In contrast, EOF2 of KCM (expl. variance: 13.5 %, Fig. 3.2(d)) represents a basinwide pattern of mostly the same sign, which is contributing most of the variance to KCM's simulated AMO index (Fig. 3.5, black line).

Comparing ERSST and KCM directly (see Fig. 3.4) shows the reason for the differences between simulated SST and observations: SST variability in the regions where the model is forced with NAO-related heat flux anomalies bear only small resemblance to observations, as denoted by correlation coefficients in the range of 0.3 to 0.5. In constrast, the regions where no heat fluxes are explained by the NAO are completely not comparable in model and observations.

All in all, this leads to the conclusion that the KCM is not able to reproduce the majority of observed spatial SST patterns as seen in the deviation from ERSST and HadISST, although it is forced by observed heat flux anomalies. The SST simulation suffers from a bias in the regions where no forcing of prescribed heat flux anomalies is applied, which presumably results as the forcing term vanishes here (see section 2.1). We may describe the bias in simple terms: The forcing is overall not strong enough to bind the simulated SST to observed SST.

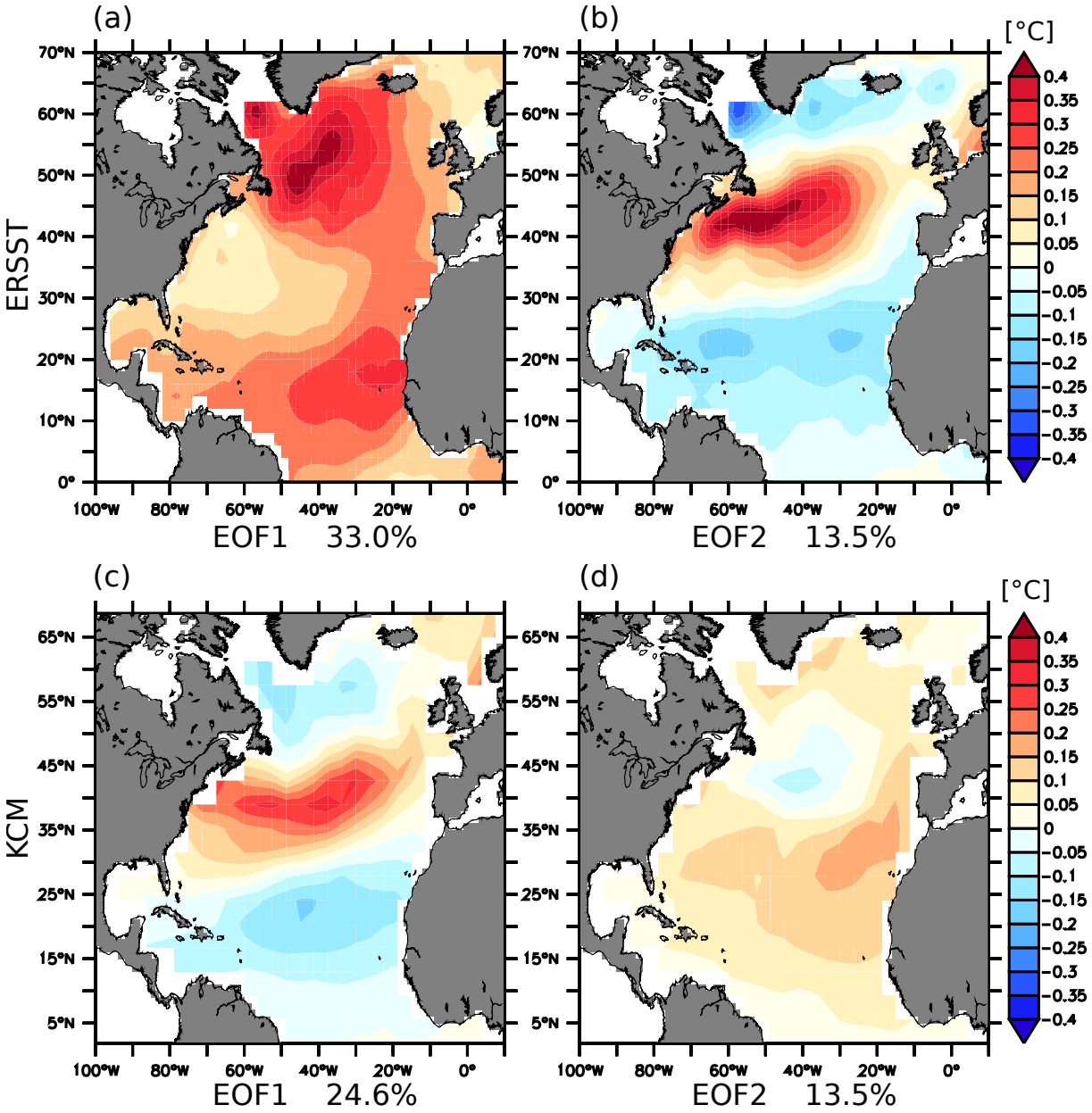

Figure 3.2: The dominant modes of SST variability as derived by the first two EOFs [°C]: (a),(b) ERSST and (c),(d) KCM ensemble mean SST. The respective explained variance is indicated directly below the pattern. (b) has been multiplied by -1 for clarity. The EOF patterns of HadISST are very similar to those of ERSST. All data has been detrended prior to analysis.

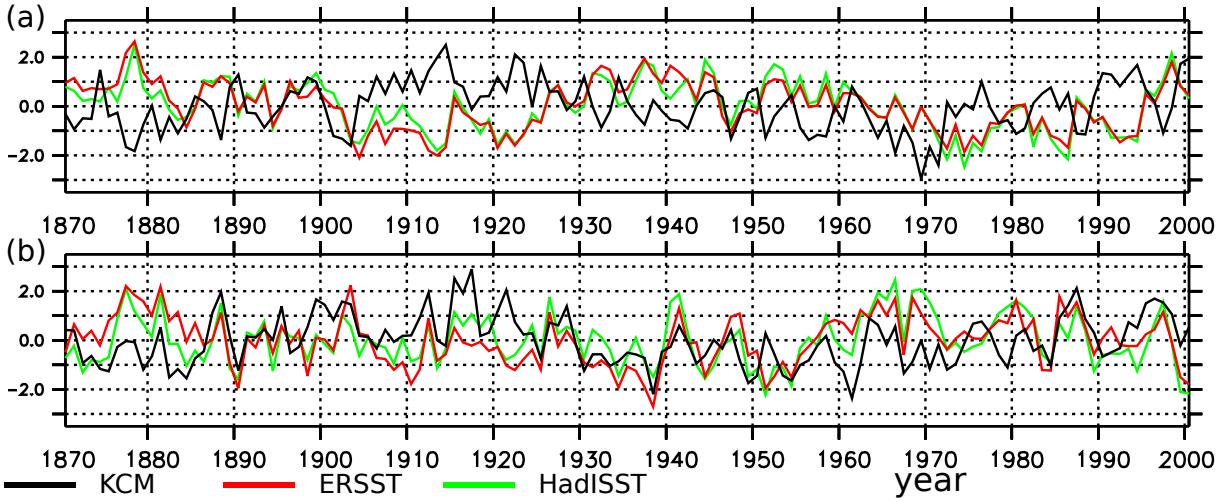

Figure 3.3: Principal Components of EOF analysis of SST in the North Atlantic (0°-70°N, 1870-2000) from ERSST, HadISST and KCM ensemble mean SST: (a) PC1, (b) PC2. PCs are dimensionless through re-normalization (section 2.2.3).

3.2 Time development - Atlantic Multidecadal Oscillation

The accuracy to reproduce twentieth century's evolution of SST variabilty in the North Atlantic is investigated by regarding the AMO index. Fig 3.5 shows the respective AMO indices calculated from ERSST, HadISST and KCM. Both reconstructed AMO indices are almost identical (correlation coefficient: 0.94), however, the AMO index resulting from the KCM ensemble mean is even negatively correlated to ERSST (coeff. -0.30) and HadISST (coeff. -0.26). Therefore, we conclude that observed and simulated AMO indices have nothing in common, leading to the result that the simulated SST is not reproducing the climate trajectory of the twentieth century North Atlantic SST variability.

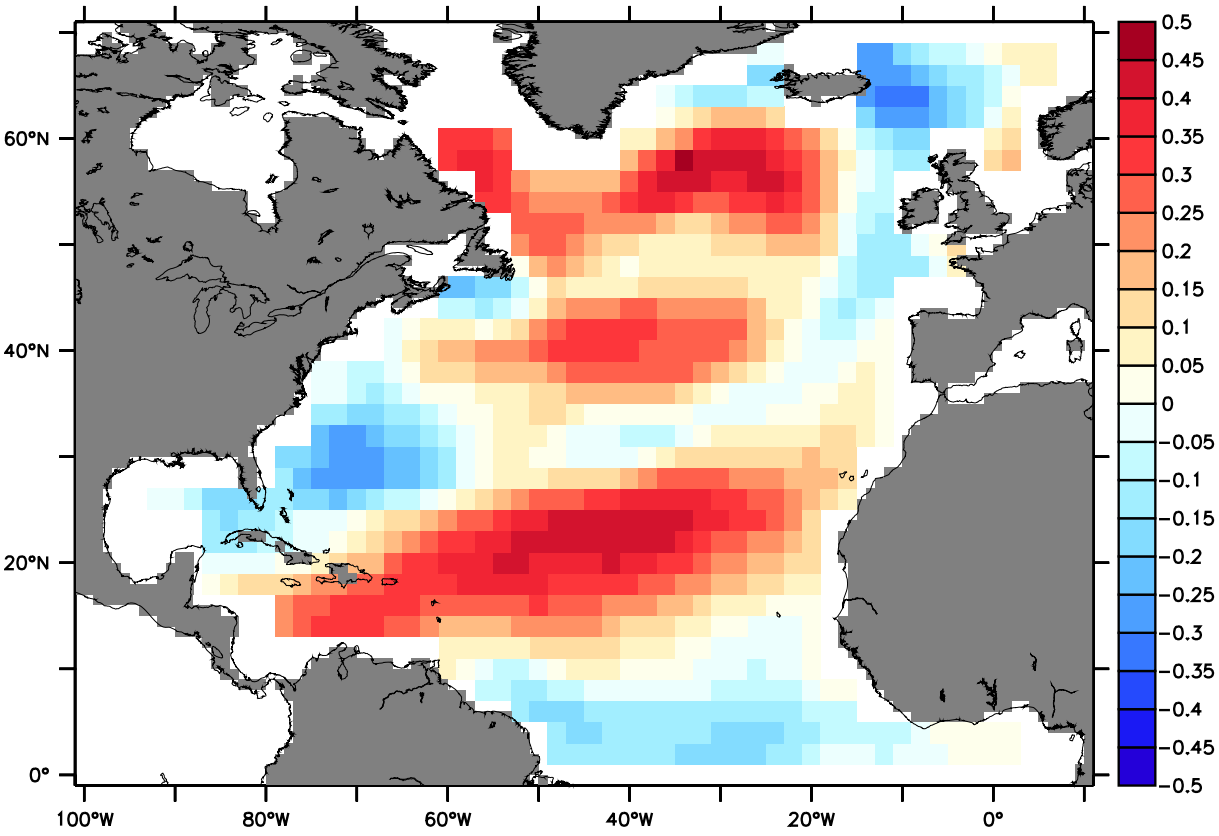

Figure 3.4: The KCM reproduces observed SST variability only in regions were observed heat flux forcing is applied: Correlation of ERSST and KCM for every grid point, seperatly. The KCM has been linearly interpolated on the ERSST grid prior to analysis. All data has been detrended prior to analysis.

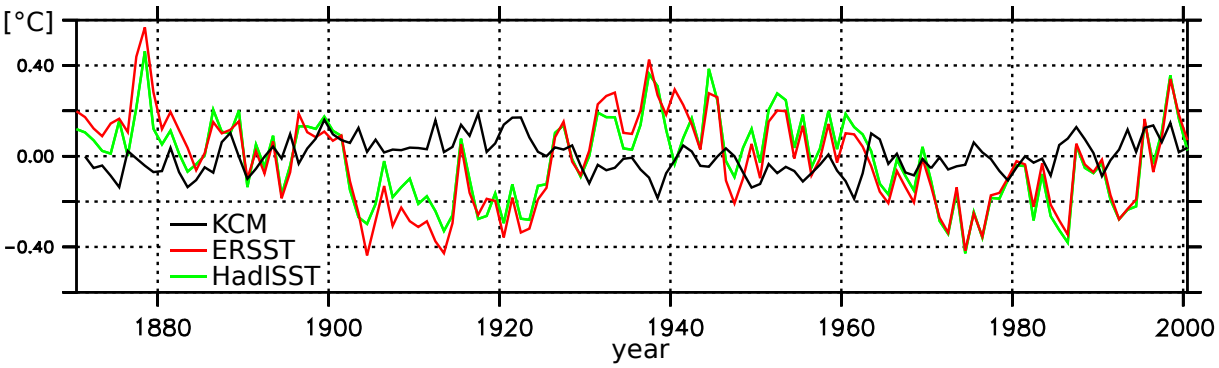

Figure 3.5: AMO index [°C] from detrended annual mean ERSST, HadISST and KCM ensemble mean SST. The index is defined as mean SST at 0-60°N in the North Atlantic. Note that ensemble mean yields smaller variance.

Chapter 4

Covariability of simulated MOC and observed SST

As presented in the last chapter, the KCM is not able to simulate SSTs comparable to observations. However, here we investigate the performance of the simulated MOC which is, in contrast, closely linked to variations in observed SST and NAO. Therefore, we use the MOC stream function instead of simulated SST to analyze the dynamic ocean's response to the NAO-related forcing.

4.1 NAO impacts the MOC

In the previous analysis we have seen that the simulated SST is directly and simultaneously affected by the NAO (Fig. 3.2(d)). In contrast, the delayed link through the overturning circulation seems not to realistically influence the ocean's surface, as the simulated AMO index does not reflect the observed SST variability (see Fig. 3.5). However, the simulated KCM ensemble mean MOC stream function (hereafter referred to simply as MOC) responds clearly to the NAO-related forcing as shown in Fig. 4.1. We regard the MOC index (maximum stream function at 30°N), as it accounts for most of the large scale variability of the MOC stream function: The covariability of NAO and MOC is indicated by an correlation coefficient of 0.74 of their respective decadal indices, if NAO is shifted 10 years ahead (significant at the 99%-level). Without shifting the coefficient is solely 0.44, denoting that variations do not occur simultaneously. This agrees well with findings of Eden & Willebrand [2001]; Latif *et al.* [2006a] and with the hypothesis of Fig. 1.4. As the link between observed NAO and simulated MOC is physically reasonable, we proceed in analyzing the spatial footprint of the MOC on the observed SST.

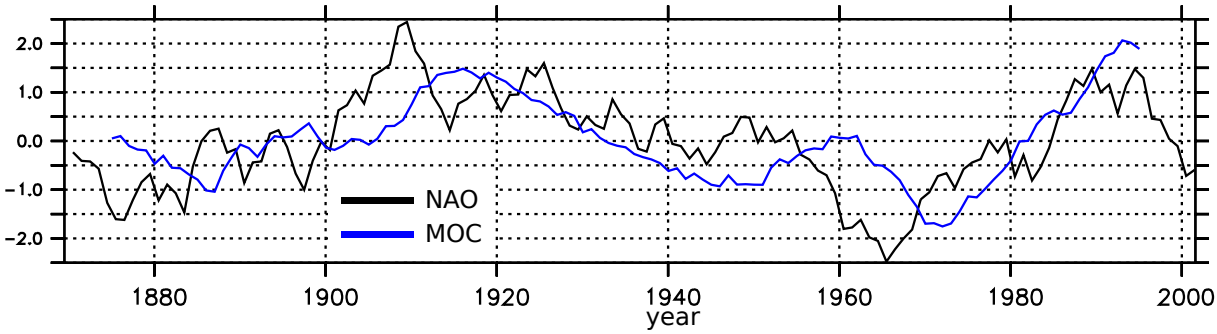

Figure 4.1: The decadal changes in the North Atlantic Oscillation show an impact on the Meridional Overturning Circulation several years later: Decadal indices of observed NAO (annual mean, station-based, see Fig. 1.2) and simulated MOC (max. stream function at 30°N). The decadal indices are calculated by the respective 11-year running means and are dimensionless through standardization. All data has been detrended prior to analysis.

4.2 Spatial footprint of the MOC

It is investigated whether the simulated MOC is statistically related to the observed SST. Fig 4.2 shows the lead-lagged explained variance of the MOC index with each grid point of ERSST. Regarding the explained variance (squared correlation, see section 2.2.6) during lag zero (Fig. 4.2(b)) shows, that changes in MOC and SST do not occur simultaneously. Indeed, shifting the MOC index 10 years ahead yields a maximum of explained variance of approximately 25% at Irminger Sea. The corresponding time series are negatively correlated with coefficients between -0.3 and -0.5 (significant at the 99%-level, not shown). Therefore, cold SSTs in the northwest North Atlantic are connected to a stronger MOC 10 years later. This mechanism is explained by the physical process of deep water formation and agrees well with findings of Eden & Jung [2001]; Eden & Willebrand [2001].

Regarding Fig. 4.2(c), (d), we identify a statistical relationship when MOC leads SST by several years. A lead of 10 years (Fig. 4.2(c)) indicates that changes in the MOC result in SST anomalies in the central North Atlantic at mid-latitudes a decade later. This connection emerges even more clearly while regarding a lead of 20 years (Fig. 4.2(d)): A positive correlation with maximum coefficients of about 0.5 (significant at the 99%-level) is located close to the gulfstream area in the western mid-latitude North Atlantic. Furthermore, the signal of explained variance is extending along the pathway of the North Atlantic current and reaching the eastern boundary at subpolar latitudes. According to Eden & Greatbatch [2003] this provides some evidence that "propagating SST anomalies" (i.e., advection of anomalous heat by mean currents, Sutton & Allen [1997]) are less important than advection of heat by anomalously strong currents, as the SST anomalies occur simultaneously.

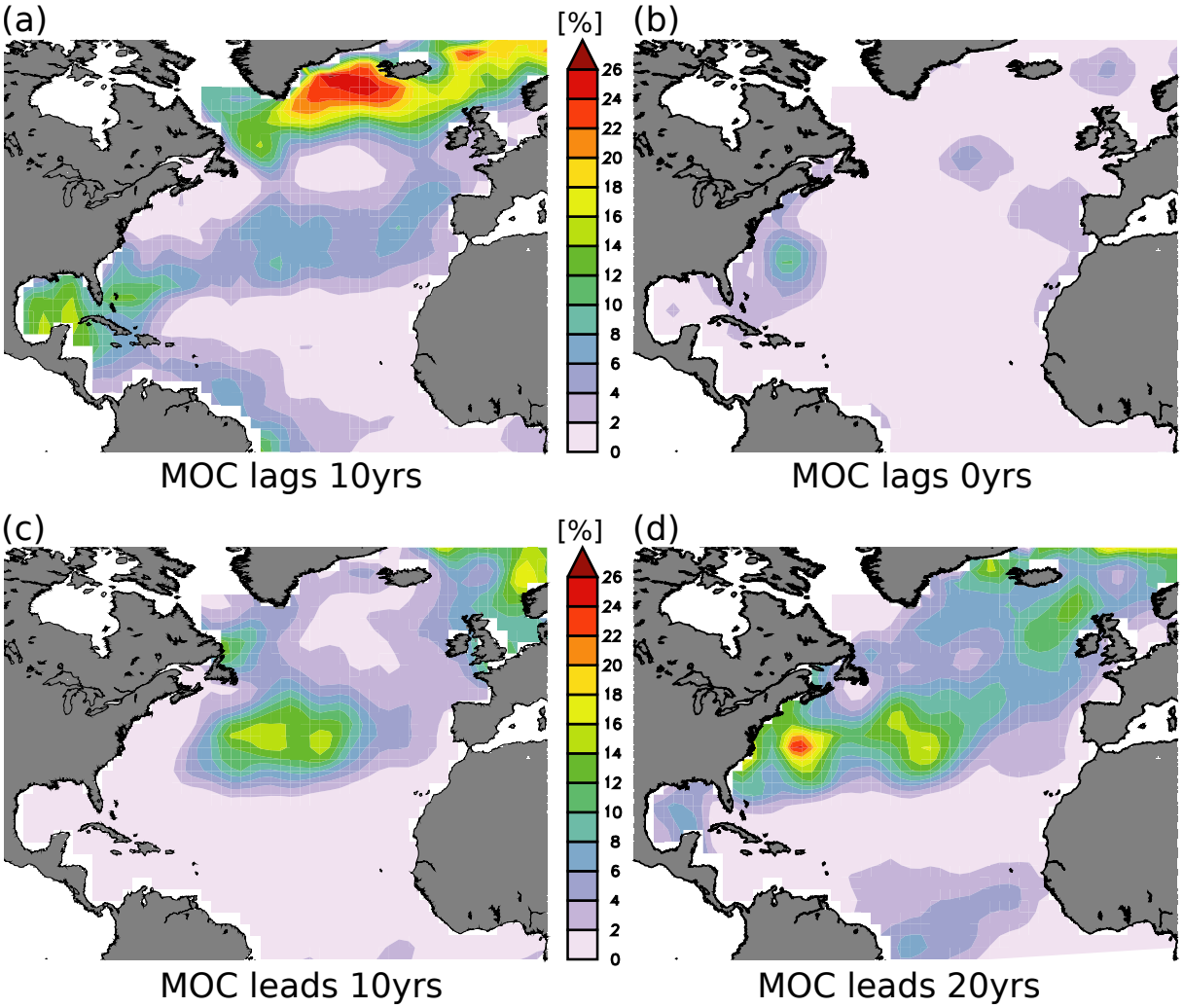

Figure 4.2: Lead-lagged spatial footprint of the Meridional Overturning Circulation. Explained variance [%] derived by the squared correlation of the MOC index (max. stream function at 30°N) with ERSST on every grid point. MOC leads SST by: (a) -10 years, (b) 0 years, (c) 10 years and (d) 20 years. All data has been detrended prior to analysis.

We conclude, that in contrast to the simulated SST the KCM shows a MOC that is statistically linked to the observed climatic evolution of the North Atlantic and therefore physically reasonable. Regarding leads and lags up to two decades it is shown, that the MOC accounts for a large amount of explained variance in the observed SST. We propose from these results that we can use the simulated MOC to investigate further, whether oceanic response signals that follow from the history of the NAO, lead to a predictive skill.

4.3 Lead-Lagged covariability of SST and MOC

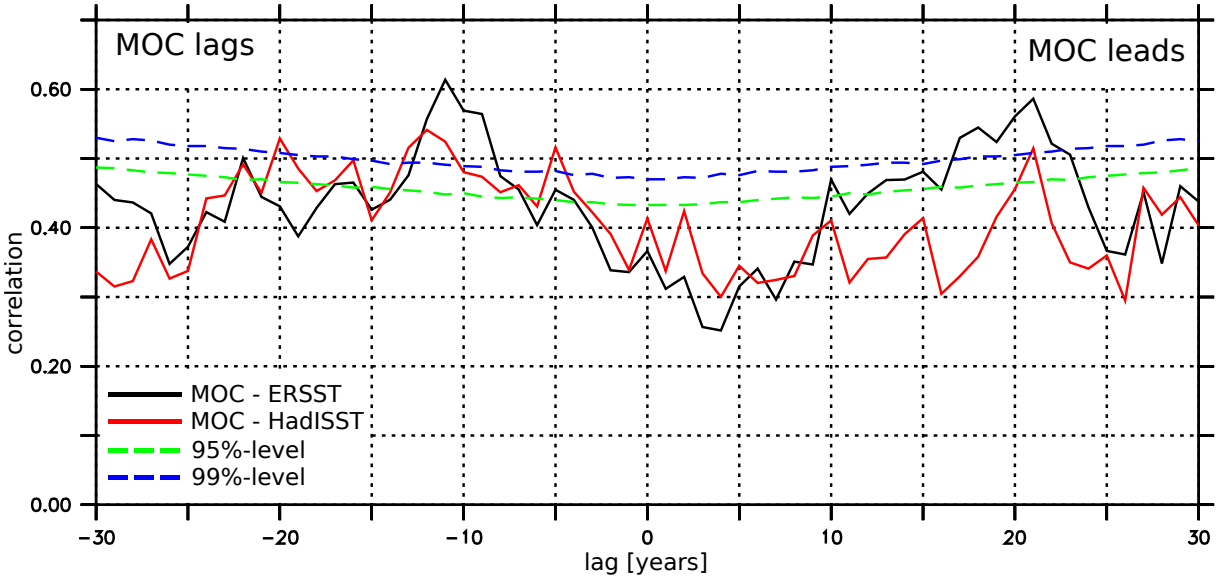

Figure 4.3: Lead-lagged correlation coefficients from 1. mode of CCA: KCM MOC ensemble mean stream function canonically correlated with (black) ERSST and (red) HadISST. CCA was performed in EOF space regarding the first five modes. Positive lag years indicate a lead of MOC, negative lag years a lead of the respective SST reconstruction. The dashed lines illustrate the respective 95% and 99%-significance levels estimated from simulations of $n = 10000$ random AR(1)-processes for every lag.

In order to investigate the covariability of observed SST and MOC Canonical Correlation Analysis (CCA, see section 2.2.4) is applied in EOF space on ERSST and MOC stream function. For CCA only the first 5 EOF modes are considered to eliminate small scale variabilities. Still, reconstructing the original field from the first 5 EOF modes explains 69% of the total variance in ERSST and MOC stream function, respectively (see Fig. 3.1(b)). The eigenvalues of the EOF transformations are shown in Fig. 3.1(a). CCA is applied shifting the time series against each other as suggested by the previous analysis of lead-lagged spatial footprints. We recognize that CCA is designed to maximize the correlation between two input variables, therefore it yields correlations even from random noise processes. Hence, it is important to investigate significance

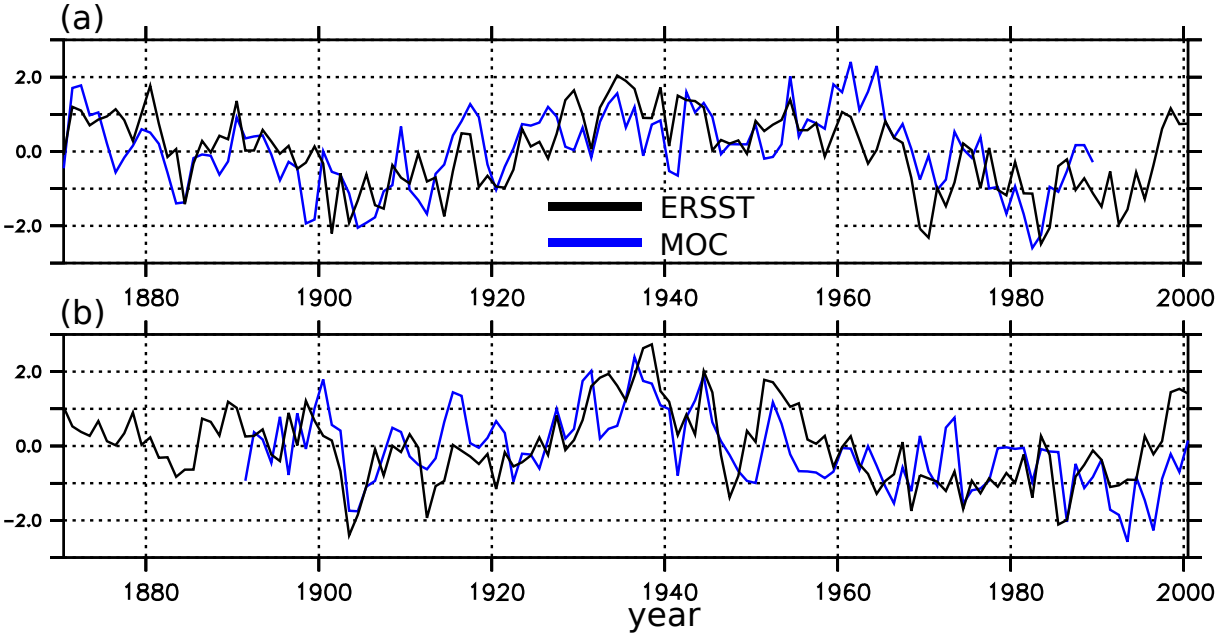

Figure 4.4: Time series of canonical variables: (a) SST leads MOC by 11 years. (b) MOC leads SST by 21 years. Since leads and lags are applied, the time axes belong to SST and the MOC time series are shifted relative to it. The associated patterns are shown in Fig. 4.5(a),(b),(c) and (d). The time series are dimensionless and (b) has been multiplied by -1 since the sign is ambiguous (according to 4.5(b), (c))

levels for CCA as described in section 2.2.7. Note that only the first CCA mode (hereafter CCA1) is considered in the present analysis.

The lead-lagged correlation coefficients for CCA1 are shown in Fig. 4.3 as a function of lag. We identify two signals that are significant at the 99%-level: First, CCA1 yields a maximum correlation of 0.61 when ERSST leads MOC by 11 years. Second, while MOC leads ERSST by 21 years the correlation is 0.59. The same analysis is performed with HadISST instead of ERSST leading to qualitatively the same results, what emphasizes the robustness. The two lead-lagged links agree well with the findings of section 4.1 and 4.2 and the associated canonical correlation patterns and time series are discussed in the following sections. For clarity, we will focus solely on ERSST, disregarding HadISST hereafter. The explained variances of all CCA modes are given in the Appendix (Tab. 1).

4.3.1 SST leads MOC by 11 years

The leading mode of CCA (CCA1) is investigated while SST leads MOC by 11 years (we will refer to this mode as *MOCLAGS*, hereafter). The canonical variables (time series) are shown in Fig. 4.4(a) and associated patterns in Fig. 4.5(a), (c) for ERSST and MOC stream function, respectively. This mode accounts for 17.4% of SST variability and 13.3% of MOC stream function

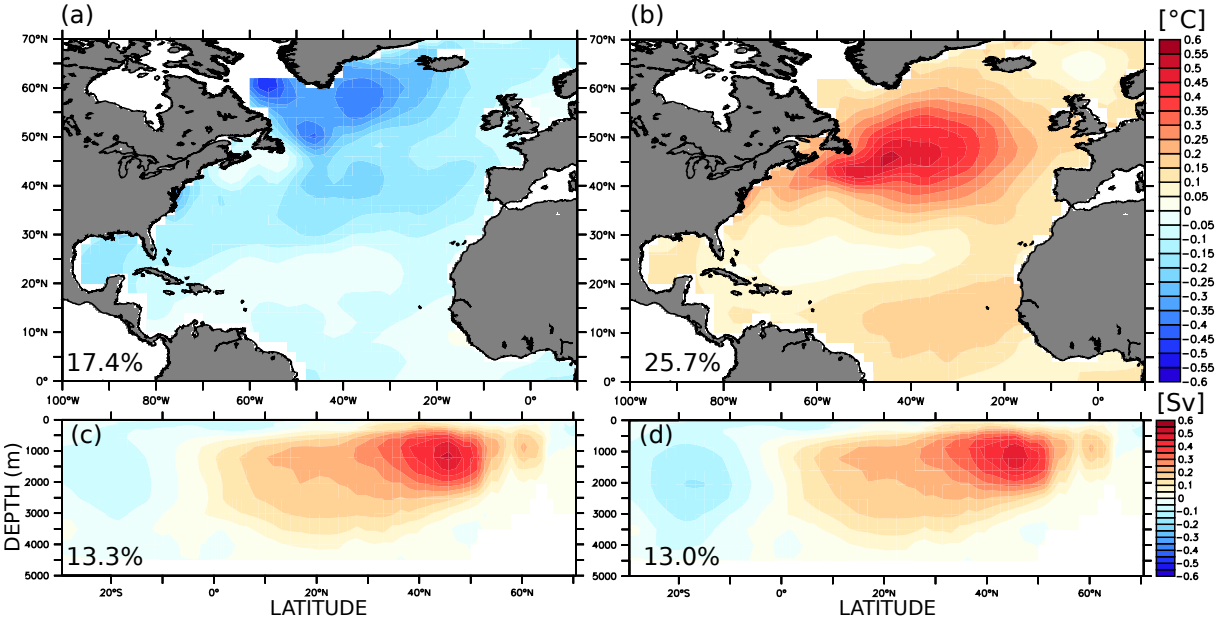

Figure 4.5: First mode of canonical correlation patterns: (a) CCA1 of ERSST for SST leads MOC by 11 years; (b) CCA1 of ERSST for MOC leads SST by 21 years; (c) CCA1 of MOC stream function for SST leads MOC by 11 years; (d) CCA1 of MOC stream function for MOC leads SST by 21 years. The explained variance is denoted in the lower left corner, respectively. Since the sign is ambiguous (b) and (d) have been multiplied by -1 for clarity. Positive values of stream function indicate clockwise overturning.

variability and their time series correlate well (0.61). Regarding Fig. 4.5(a) we see a negative SST anomaly of -0.6 °C in Labrador Sea and Irminger Sea which is linked to an intensification of 0.5 Sv of the MOC at 50°N (Fig. 4.5(c)) 11 years later. The time series (Fig. 4.4(a)) mainly reflect the multi-decadal variations of the observed AMO index (Fig. 3.5) indicated by correlation coefficients of 0.31 to ERSST and 0.52 to MOC (significant at the 99%-level). Hence, we connect *MOCLAGS* to the physical process of deep water formation in Labrador Sea and Irminger Sea and a delayed response of the MOC through its intensification.

4.3.2 MOC leads SST by 21 years

In the following the leading mode of CCA is investigated while MOC leads SST by 21 years (we will refer to this mode as *MOCLEADS*, hereafter). The canonical variables (time series) are shown in Fig. 4.4(b) and associated patterns in Fig. 4.5(b), (d) for ERSST and MOC stream function, respectively. This mode accounts for 25.7% of SST variability and 13.0% of MOC stream function variability and their time series correlate well (0.59). Regarding the time series (Fig. 4.4(b)), we identify that the low-frequency variations of *MOCLEADS* are thoroughly comparable to those of the canonical variables of *MOCLAGS* (Fig. 4.4(a)). Hence, it is supposed

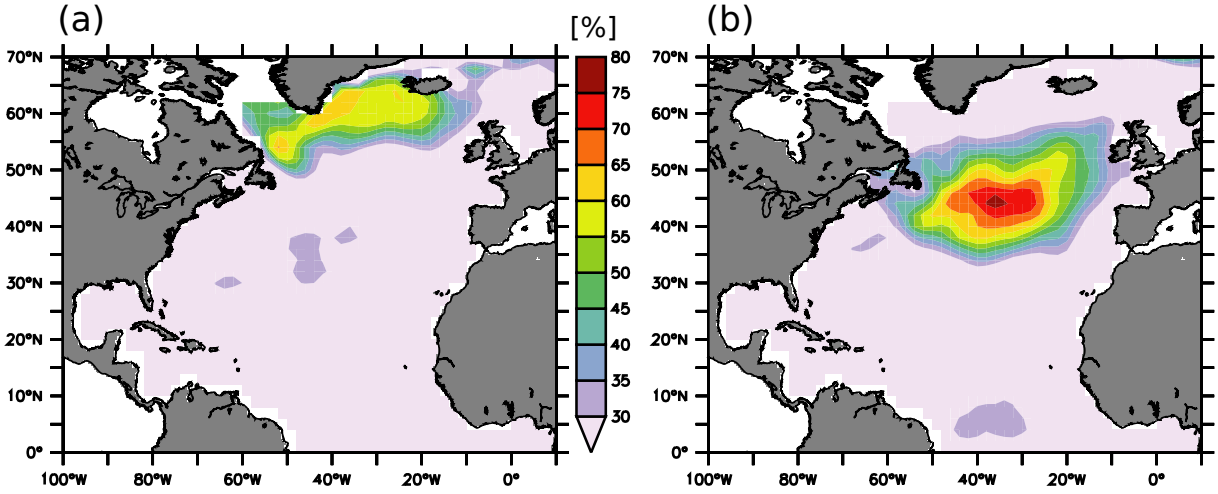

Figure 4.6: Locally explained variance [%] of SST reconstructed from CCA1: (a) SST leads MOC by 11 years, (b) MOC leads SST by 21 years. CCA was performed as described in caption of Fig. 4.3.

that these two CCA1 modes are closely connected to each other. This assumption is confirmed while comparing the canonical correlation patterns of MOC stream function (Fig. 4.5(c) and (d)) as both patterns are nearly identical. This suggests that the same linear combination of MOC modes is connected to: (i) cold SSTs in the sinking regions 11 years before and (ii) positive SST anomalies of about 0.6°C located at the northward end of the gulfstream area and spreading out in the North Atlantic between 40° and 60°N (Fig. 4.5(b)). Furthermore, we see that the centers of action in the canonical correlation patterns (Fig. 4.5(a), (b)) of *MOCLAGS* and *MOCLEADS* are in coincidence with the respective areas of most explained variance (Fig. 4.6). Hence, both modes indeed represent most of the local SST variability. Altough, the centers of action of *MOCLAGS* and *MOCLEADS* are not the same, we assume that the positive anomalies in the mid-latitude North Atlantic (Fig. 4.5(b)) are going to replace the negative anomalies in the subpolar North Atlantic (Fig. 4.5(a)) several years later, following the path of the subpolar gyre circulation [Schmitz & McCartney, 1993; Sutton & Allen, 1997]. Thus, adding up the lags of both CCA modes, we identify a negative feedback whose half-cycle lasts at least three decades: the AMO. However, it is still unclear whether (i) the negative feedback is actually realized through propagating SST anomalies, or (ii) how the ocean feeds back onto the NAO. It should be mentioned that the feedback here is statistically identified and do not provide any evidence about its physical mechanisms.

Chapter 5

Prediction of SST until 2021

Following the results of the last chapter simulated MOC variations are closely related to observed SST variations two decades later, according to the AMO. Thus, we proceed in using the simulated MOC, which is available until 2000, as predictor for SST until 2021.

5.1 CCA as predictive tool

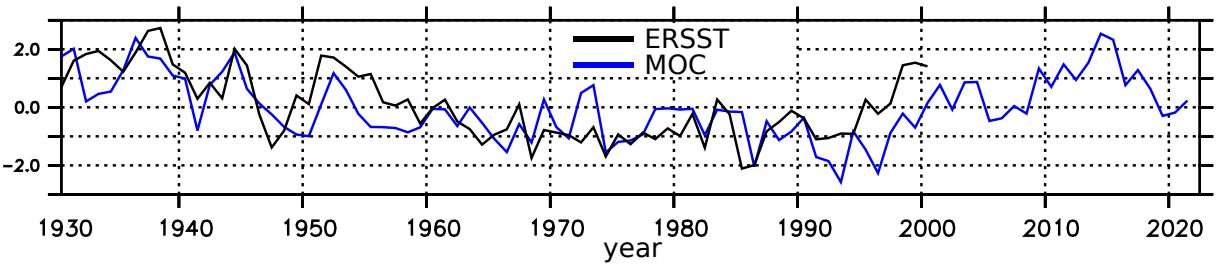

Figure 5.1: Extension of canonical variables of CCA1 from Fig. 4.4(b) until 2021. Since the MOC stream function is simulated until 2000 and leads SST by 21 years the linear combination of its PCs according to CCA1 is used to predict SST variability until 2021. The time series are dimensionless.

We recognize that CCA can be used as a predictive tool, since leads and lags are involved. Considering the *MOCLEADS* mode we define MOC as predictor and SST as predictand. Hence, the linear combination of the MOC stream function PCs yields a time series which is an estimator for the corresponding SST time series, since both are designed for most correlation. The MOC stream function is simulated until 2000, thus we apply the same linear combination on the PCs from 1980-2000 yielding a time series that is supposed to correlate most with its associated SST time series from 2001-2021. Fig. 5.1 shows the extended canonical variable of Fig. 4.4(b). Therefore, we use the canonical variable of MOC stream function as an estimator for the canonical variable of SST. Given the canonical correlation pattern of SST we are able to "reconstruct"

(the future as well as the past) the SST variability in the North Atlantic by multiplying the canonical variable of MOC stream function (Fig. 5.1, blue) with the canonical correlation pattern of SST (Fig. 4.5(b)). The result is an SST prediction for the period of 2001-2021. It should be mentioned, that the prediction may be performed including higher modes of CCA, though not done in this study.

5.2 North Atlantic SST cooling after 2015

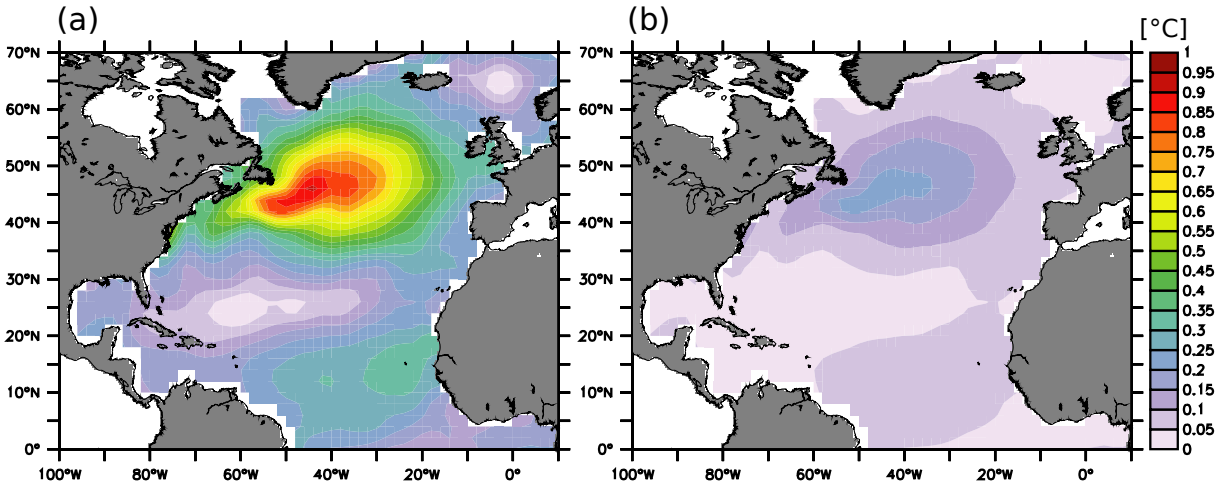

Figure 5.2: SST anomaly predicition with CCA1: (a) Mean SST anomaly for 2011-2015, (b) mean SST anomaly for 2016-2020. The anomalies are relative to the 1870-2000 climatology. Since there are no negative anomalies to illustrate, the colobar does not include negative values for clarity.

The AMO is currently in a positive phase of its 60- to 70-year cycle, as seen in Fig. 5.3 (we extended the ERSST data set here until 2012 for comparison, as indicated in red). The SST prediction based on CCA leads to the following conclusion considering the future development until 2021: The positive SST anomalies in the North Atlantic retain in the first half of the current decade as shown in Fig. 5.2(a) by the mean anomly during 2011-2015. In contrast, shown in Fig. 5.2(b), the anomalies decrease for the second half of the current decade, as denoted by a state, which follows more closely the climatology from 1870 to 2000. Furthermore, the AMO index (Fig. 5.3, blue) can be reconstructed for the last century as well as predicted until 2021, by means of the same CCA-based method resulting solely from the simulated MOC stream function. In comparison to the observed AMO index, we identify that our reconstruction follows closely the decadal variations, which is quantified by a correlation coefficient of 0.59 for the illustrated period (1930-2012). While applying an 11-year running mean the higher coefficient of 0.73 emphasizes that our prediction/reconstruction reflects mostly the (multi-)decadal variability

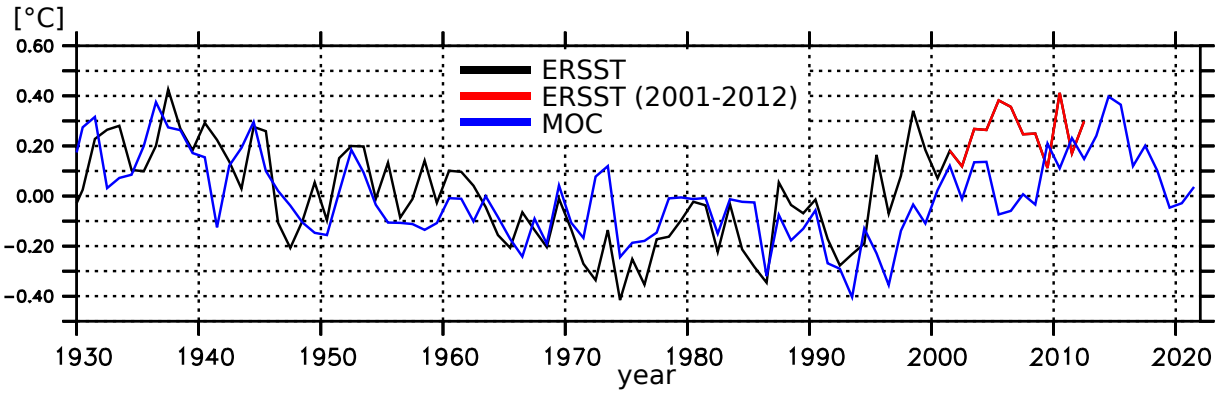

Figure 5.3: Prediction of AMO index until 2021. Since MOC leads SST by 21 years CCA1 allows a reconstruction of the SST variability from canonical variables and patterns leading to the AMO index as shown in blue. The observed AMO index results from ERSST (black). Additionally, the period 2001-2012 (red) was not used for the present analysis, still, as available from ERSST shown for comparison.

of the observed AMO index. Indeed, the period of 2001-2012, which was not included in the present analysis, suggests that the predicition on annual time scales is still far from satisfactory. However, on decadal time scales this method leads to an AMO index for the next two decades that is supposed to correlate well with the observations. Furthermore, we conclude to expect North Atlantic SST cooling after 2015, which is physically reasonable as the latest high phase of the simulated MOC has been in the years 1993-1996 (Fig. 4.1). During the next years further studies would need to compare this to observations.

Chapter 6

Concluding discussion

6.1 Conclusions

We have considered a coupled climate model to investigate whether the MOC leads to a predictive skill for North Atlantic SST variability. The model is forced with observed NAO-related heat flux anomalies in order to produce a MOC that is consistent with the decadal changes of North Atlantic climate during the twentieth century. Our findings are in summary concluded as follows:

(i) It is shown that the simulated MOC is closely following the decadal changes of the NAO. Of particular interest is the statistical relation between MOC and observed SST: Decadal changes in the subpolar North Atlantic as well as in the North Atlantic Current (NAC) region are consistent with the simulated MOC in a sense that: Subpolar SST anomalies have been detected to appear 11 years later in the MOC and in turn, another 21 years later in the NAC region. The negative feedback resulting from this relationship has been associated with the AMO and is physically reasonable.

(ii) However, the KCM suffers from errors as the simulated SST is, apart from the regions where the NAO explains heat flux anomalies, thoroughly not comparable to observations.

(iii) Statistical investigations with CCA provide perspectives for predicting North Atlantic decadal SST variability. Though, we recognize that interannual changes are far from being predictable by means of heat flux forcing. CCA proposes a technique to forecast SSTs 21 years ahead based on the simulated MOC. Following this method, North Atlantic SST cooling has to be expected from 2015 onwards, which physically results from the simulated MOC weakening since the mid 1990's.

Eden & Jung [2001] proposed, with their idea to force a model with NAO-related heat fluxes, a method to simulate a consistent MOC that clearly reacts on subpolar heat flux anomalies. In summary, combining their method and the results of this study it is possible to extend the prediction of North Atlantic SST regularly, provided solely that the observed NAO index is available. As an outlook, we are looking forward to extend the experiment from 2000 to the near past.

6.2 Discussions

Finally, it is necessary to discuss critically the results of the present analysis. Throughout the thesis the term "realistic" is avoided to describe the simulated MOC for several reasons. One has to recognize that observational records for the ocean, apart from the sea surface, are very restricted. Hence, classifying a simulated MOC as "reaslistic" causes problems, as the true state of the deep circulation during the last century is unkown. However, some recent efforts have been carried out to reach a consensus about the current state of the MOC, including observations (RAPID MOC monitoring array since 2004, Cunningham *et al.* [2007]; Kanzow *et al.* [2007]) and data assimilation projects [Balmaseda *et al.*, 2010, 2013].

Nevertheless, the uncertainties about the MOC during the last decades remain, emphasized in Fig. 6.1: Different ocean models (with and without data assimiliation) are simulating completely different evolution of the MOC index (at 26°N for comparison with RAPID). Additionally, a large unclarity about the future development prevails: As shown by Weaver *et al.* [2012] many climate models simulate a weaking of the MOC for the next few decades due to climate change. But apart from this common feature, the models differ largely in mean value, variability and stability of the MOC.

Of particular importance for this study is the fact, that even though the here simulated MOC is consistent with the forcing as well as with the observed SST, there is no way to assess this simulation. We are therefore not able to describe our MOC as "realistic". Every ensemble member is one possible realization of the MOC, including the discrepancies of the model in comparison to reality. Considering the ensemble mean, one may even regard it as "statistical construct" that possibly has nothing in common with reality. Nevertheless, eliminating the chaotic behaviour of every ensemble member by averaging yields a MOC that follows an idealized climatic trajectory. Not a trajectory that is realisitic, but one that represents an estimate for the state of the MOC only due to its heat flux forcing. So bearing this difference in mind, the present study is reasonable as we provide an estimate for the future state of North Atlantic SST, which is idealized in its relationship to the previous state of the NAO.

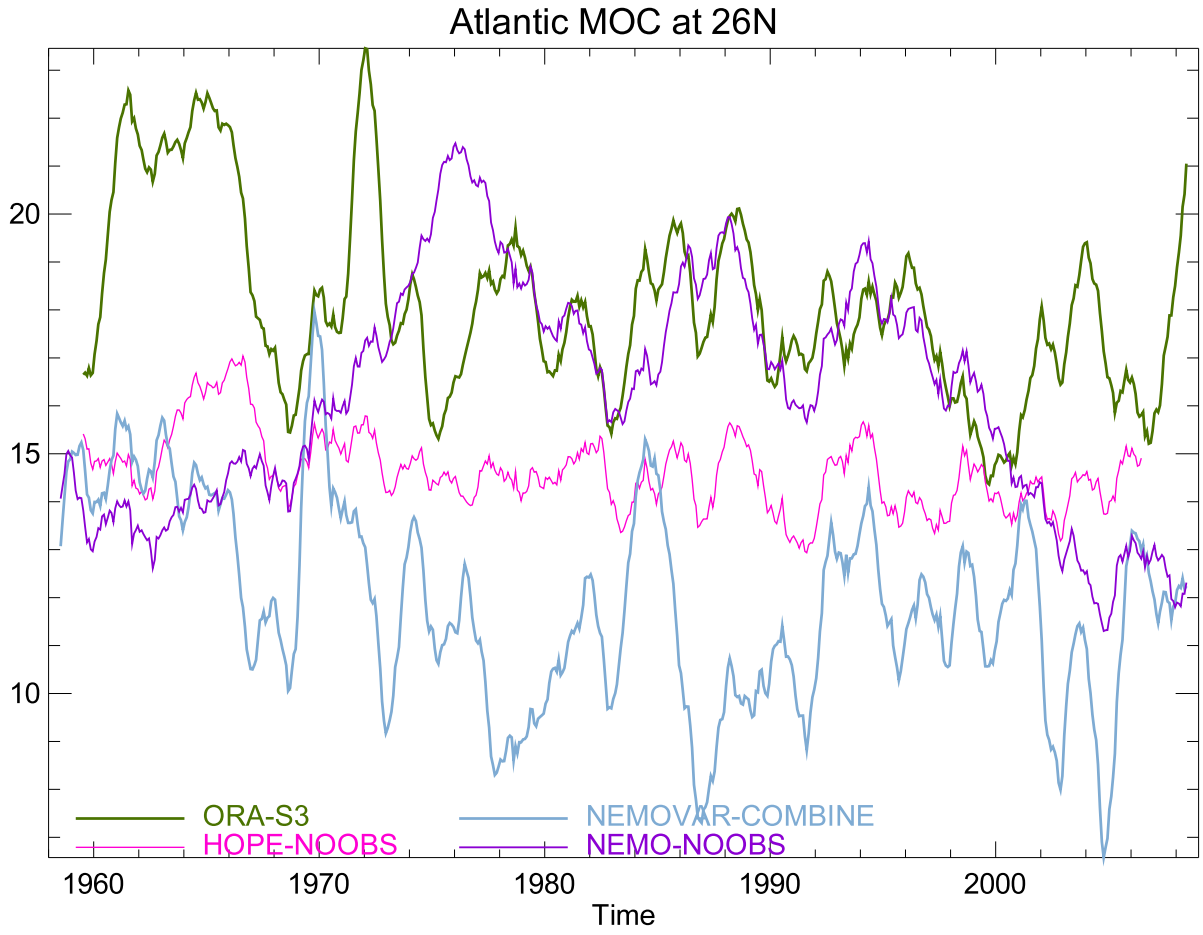

Figure 6.1: The unknown state of the Atlantic Meridional Overturning Circulation during the last decades. MOC [Sv] at 26°N as represented by ocean reanalyses: ORAS3 (green), NEMOVAR (blue); and the same ocean models without assimilated obeservations: HOPE-NOOBS (pink) and NEMOVAR-NOOBS (violet). All models are forced with observed surface fluxes from ERA reanalyses. From Balmaseda *et al.* [2010].

Appendix

.1 Statistical nomenclature

Variance

The variance is a way to measure the deviation of a random variable X from its expected value μ.

$$\mathrm{Var}(X) = \mathcal{E}\left((X-\mu)^2\right) \tag{1}$$

Similarly, we define the variance of a vector $\vec{X}$ as the sum over all variances of the elements X_i

$$\mathrm{Var}(\vec{X}) = \sum_i \mathcal{E}\left((X_i-\mu_i)^2\right) \tag{2}$$

Covariance

The covariance σ of two univariate random variables X, Y is a measurement to quantify whether X, Y vary jointly

$$\sigma = \mathrm{Cov}(X,Y) = \mathcal{E}\left((X-\mu_X)(Y-\mu_Y)\right). \tag{3}$$

Covariance matrix

Regarding two random vectors $\vec{X}, \vec{Y}$ the covariance matrix $\Sigma_{\vec{X},\vec{Y}}$ is defined as

$$\Sigma_{\vec{X},\vec{Y}} = \mathrm{Cov}(\vec{X},\vec{Y}) = \mathcal{E}\left((\vec{X}-\vec{\mu_X})(\vec{Y}-\vec{\mu_Y})^T\right). \tag{4}$$

where the superscript T denotes that that the assigned vector has been transposed. Hence, the covariance

$$\sigma_{i,j} = \mathcal{E}\left((X_i-\mu_{X_i})(Y_j-\mu_{Y_j})\right) \tag{5}$$

is the (i,j)th element of $\Sigma_{\vec{X},\vec{Y}}$. The sample covariance matrix $\hat{\Sigma}$ is estimated from samples $\{\vec{x}_1,...,\vec{x}_n\},\{\vec{y}_1,...,\vec{y}_n\}$ of realizations of $\vec{X},\vec{Y}$ as follows

$$\hat{\Sigma}_{i,j} = \frac{1}{n}\sum_{k=1}^{n}(x_{i,k}-\bar{x}_i)(y_{j,k}-\bar{y}_j) \tag{6}$$

where i,j refers to the (i,j)th element of $\hat{\Sigma}$. $\bar{x},\bar{y}$ is the respective mean.

.2 Supplementary figures and tables

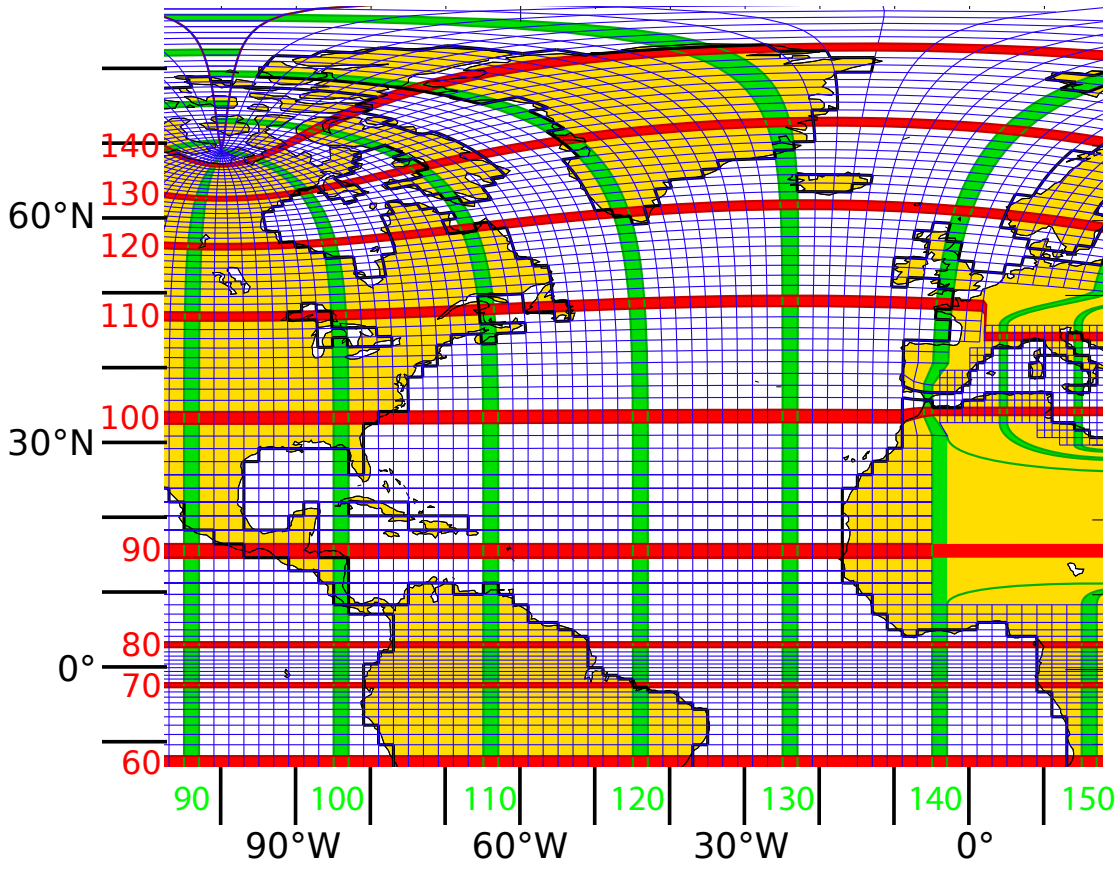

Figure 2: The tripolar ORCA2 grid that was used for OPA9, the ocean component of the Kiel Climate Model. One of the poles is located in North Canada, the other one in Siberia, wich leads to no singularity at the North Pole. The equatorial refinement allows a better representation of equatorial processes. The green line crossing iceland is the zonal grid cell index 130, which was used to reassign the MOC stream function with latitudes.

	MOCLEADS		*MOCLAGS*	
CCA mode	ERSST	MOC	ERSST	MOC
1	25.7	13.0	17.4	13.3
2	11.3	15.4	10.5	16.0
3	11.8	14.7	13.9	11.3
4	9.4	14.4	13.6	14.9
5	8.8	11.3	13.4	13.3
Σ	67.0	68.8	68.8	68.9

Table 1: Explained variance of CCA modes given in %. The accumulated explained variance is indicated by Σ, exact equality to the accumulated explained variance of EOF is not given due to computational errors. *MOCLAGS* (*MOCLEADS*) refer to SST leads MOC by 11 years (MOC leads SST by 21 years). Calculated from equation 2.24.

Acknowledgements

I would like to acknowledge climate data from the following institutions

- NOAA/NESDIS/National Climatic Data Center for providing their NOAA Extended Reconstructed SST V3b,
- Met Office, Hadley Centre for Climate Research for providing their Hadley Centre Global Sea Ice and Sea Surface Temperature (HadISST) v1.1,
- James Hurrel and the Climate Analysis Section, NCAR, Boulder, USA, for providing their Hurrell North Atlantic Oscillation (NAO) Index (station-based).

Additionally, I wish to acknowledge

- NOAA Pacific Marine Environmental Laboratory for providing their data visualization and analysis programme Ferret v6.8.2,
- Max-Planck-Institute for Meteorology for providing their tool set Climate Data Operators (CDO) v1.5.9,
- Harish Bhanderi, Cambridge University, for providing a LaTeX-template, which was used for this thesis in a modified version,
- and the Buffalo Club for the awareness, that a right-hand glove could be put on a left hand if it could be turned round in four-dimensional space.

References

Álvarez García, F., Latif, M. & Biastoch, A. (2008). On Multidecadal and Quasi-Decadal North Atlantic Variability. *J. Climate*, **21**, 3433–3452. 3

Balmaseda, M.A., Mogensen, K., Molteni, F. & Weaver, A.T. (2010). The NEMOVAR-COMBINE ocean re-analysis. Tech. Rep. 1, COMBINE. 31, 32

Balmaseda, M.A., Mogensen, K. & Weaver, A.T. (2013). Evaluation of the ECMWF ocean reanalysis system ORAS4. *Q. J. R. Meteorol. Soc.*. 31

Barnett, T.P. & Preisendorfer, R. (1987). Origins and Levels of Monthly and Seasonal Forecast Skill for United States Surface Air Temperatures Determined by Canonical Correlation Analysis. *Mon. Wea. Rev.*, **115**, 1825–1850. 12

Bjerknes, J. (1964). Atlantic air sea interaction. *Advances in Geophysics*, **10**, 1–82. 1, 4

Broecker, W. (1991). The great ocean conveyor. *Oceanography*, **4**, 79–89. 1

Cunningham, S.A., Kanzow, T., Rayner, D., Baringer, M.O., Johns, W.E., Marotzke, J., Longworth, H.R., Grant, E.M., Hirschi, J.J.M., Beal, L.M., Meinen, C.S. & Bryden, H.L. (2007). Temporal Variability of the Atlantic Meridional Overturning Circulation at 26.5°N. *Science*, **317**, 935–938. 31

Delworth, T.L. & Greatbatch, R.J. (2000). Multidecadal Thermohaline Circulation Variability Driven by Atmospheric Surface Flux Forcing. *J. Climate*, **13**, 1481–1495. 2, 4

Dima, M. & Lohmann, G. (2007). A Hemispheric Mechanism for the Atlantic Multidecadal Oscillation. *J. Climate*, **20**, 2706–2719. 4

Eden, C. & Greatbatch, R. (2003). A Damped Decadal Oscillation in the North Atlantic Climate System. *J. Climate*, **16**, 4043–4060. 3, 4, 21

Eden, C. & Jung, T. (2001). North Atlantic Interdecadal Variability: Oceanic Response to the North Atlantic Oscillation (1865–1997). *J. Climate*, **14**, 676–691. 2, 3, 4, 5, 7, 15, 21, 30

Eden, C. & Willebrand, J. (2001). Mechanism of Interannual to Decadal Variability of the North Atlantic Circulation. *J. Climate*, **14**, 2266–2280. 2, 3, 4, 12, 20, 21

Emery, W.J. & Thomson, R.E. (2001). *Data Analysis Methods in Physical Oceanography*. Elsevier, 2nd edn. 8

Getzlaff, J., Böning, C.W., Eden, C. & Biastoch, A. (2005). Signal propagation related to the North Atlantic overturning. *Geophys. Res. Lett.*, **32**. 4

Grist, J.P., Marsh, R. & Josey, S.A. (2009). On the Relationship between the North Atlantic Meridional Overturning Circulation and the Surface-Forced Overturning Streamfunction. *J. Climate*, **22**, 4989–5002. 2

Hall, M.M. & Bryden, H.L. (1982). Direct estimates and mechanisms of ocean heat transport. *Deep-Sea Res.*, **29A**, 339–359. 1

Hotteling, H. (1935). The most predictable criterion. *J. Ed. Psych.*, **26**, 139–142. 10

Hotteling, H. (1936). Relations between two sets of variants. *Biometrika*, **28**, 321–377. 11

Hurrell, J.W. (1995). Decadal Trends in the North Atlantic Oscillation: Regional Temperatures and Precipitation. *Science*, **269**, 676–679. 2, 4, 7, 16

Hurrell, J.W. & Deser, C. (2010). North Atlantic climate variability: The role of the North Atlantic Oscillation. *Journal of Marine Systems*, **79**, 231–244. 2

Kalnay, E., Kanamitsu, M., Kistler, R., Collins, W., Deaven, D., Gandin, L., Iredell, M., Saha, S., White, G., Woollen, J., Zhu, Y., Leetmaa, A., Reynolds, R., Chelliah, M., Ebisuzaki, W., Higgins, W., Janowiak, J., Mo, K.C., Ropelewski, C., Wang, J., Jenne, R. & Joseph, D. (1996). The NCEP/NCAR 40-Year Reanalysis Project. *Bull. Amer. Meteor. Soc.*, **77**, 437–471. 7

Kanzow, T., Cunningham, S.A., Rayner, D., Hirschi, J.J.M., Johns, W.E., Baringer, M.O., Bryden, H.L., Beal, L.M., Meinen, C.S. & Marotzke, J. (2007). Observed Flow Compensation Associated with the MOC at 26.5°N in the Atlantic. *Science*, **317**, 938–941. 31

Kerr, R.A. (2000). A North Atlantic climate pacemaker for the centuries. *Science*, **288**, 1984–1985. 3

Kushnir, Y. (1994). Interdecadal Variations in North Atlantic Sea Surface Temperature and Associated Atmospheric Conditions. *J. Climate*, **7**, 141–157. 1

Latif, M., Arpe, K. & Roeckner, E. (2000a). Oceanic Control of Decadal North Atlantic Sea Level Pressure Variability in Winter. *Geophys. Res. Lett.*, **27**, 727–730. 3, 4, 12, 15

Latif, M., Roeckner, E., Mikolajewicz, U. & Voss, R. (2000b). Tropical Stabilization of the Thermohaline Circulation in a Greenhouse Warming Simulation. *J. Climate*, **13**, 1809–1813. 9

Latif, M., Roeckner, E., Botzet, M., Esch, M., Haak, H., Hagemann, S., Jungclaus, J., Legutke, S., Marsland, S., Mikolajewicz, U. & Mitchell, J. (2004). Reconstructing, Monitoring, Predicting Multidecadal-Scale Changes in the North Atlantic Thermohaline Circulation with Sea Surface Temperature. *J. Climate*, **17**, 1605–1614. 4

Latif, M., Böning, C., Willebrand, J., Biastoch, A., Dengg, J., Keenlyside, N., Schweckendiek, U. & Madec, G. (2006a). Is the Thermohaline Circulation Changing? *J. Climate*, **19**, 4631–4637. 3, 9, 20

Latif, M., Collins, M., Pohlmann, H. & Keenlyside, N. (2006b). A Review of Predictability Studies of Atlantic Sector Climate on Decadal Time Scales. *J. Climate*, **19**, 5971–5987. 2, 4, 5

Lorenz, E. (1956). Empirical orthogonal functions and statistical weather prediction. Statistical forecast project report 1, Dept. of Meteor., MIT, 49pp. 10

Madec, G. (2008). NEMO ocean engine. *Note du Pole de modélisation*, **27**, institut Pierre-Simon Laplace, 193 pp. 6

Menary, M., Park, W., Lohmann, K., Vellinga, M., Palmer, M., Latif, M. & Jungclaus, J. (2012). A multimodel comparison of centennial Atlantic meridional overturning circulation variability. *Clim. Dyn.*, **38**, 2377–2388. 9

Olbers, D., Willebrand, J. & Eden, C. (2012). *Ocean Dynamics*. Springer, 704 p. 14

Park, W. & Latif, M. (2008). Multidecadal and multicentennial variability of the meridional overturning circulation. *Geophys. Res. Lett.*, **35**, 1–5. 9

Park, W. & Latif, M. (2012). Atlantic Meridional Overturning Circulation response to idealized external forcing. *Clim. Dyn.*, **39**, 1709–1726. 9

Park, W., Keenlyside, N., Latif, M., Ströh, A., Redler, R., Roeckner, E. & Madec, G. (2009). Tropical Pacific Climate and Its Response to Global Warming in the Kiel Climate Model. *J. Climate*, **22**, 71—-92. 6

Pearson, K. (1902). On lines and planes of closest fit to systems of points in space. *Phil. Mag.*, **2**, 559–572. 10

Pohlmann, H., Sienz, F. & Latif, M. (2006). Influence of the Multidecadal Atlantic Meridional Overturning Circulation Variability on European Climate. *J. Climate*, **19**, 6062–6067. 1

Rayner, N.A., Parker, D.E., Horton, E.B., Folland, C.K., Alexander, L.V., Rowell, D.P., Kent, E.C. & Kaplan, A. (2003). Global analyses of sea surface temperature, sea ice, and night marine air temperature since the late nineteenth century. *J. Geophys. Res.*, **108**, No. D14, 4407. 8, 9

Roeckner, E., Bäuml, G., Bonaventura, L., Brokopf, R., Esch, M., Giorgetta, M., Hagemann, S., Kirchner, I., Kornblueh, L., Manzini, E., Rhodin, A., Schlese, U., Schulzweida, U. & Tompkins, A. (2003). The atmospheric general circulation model ECHAM5. Part I: Model description. *Max Planck Institute for Meteorology Rep.*, **349**, 127 pp. 6

Schlesinger, M.E. & Ramankutty, N. (1994). An oscillation in the global climate system of period 65–70 years. *Nature*, **367**, 723–726. 3, 15

Schlesinger, M.E. & Ramankutty, N. (1995). Is the recently reported 65- to 70-year surface-temperature oscillation the result of climatic noise? *J. Geophys. Res.*, **100**, 13767–13774. 3, 15

Schmitz, W.J. & McCartney, M.S. (1993). On the North Atlantic Circulation. *Rev. of Geophys*, **31**, 29–49. 26

Smith, T., Reynolds, R., Peterson, T.C. & Lawrimore, J. (2008). Improvements to NOAA's Historical Merged Land-Ocean Surface Temperature Analysis (1880-2006). *J. Climate*, **21**, 2283–2296. 7, 8, 9

Stewart, R.H. (2008). *Introduction to Physical Oceanography*. Department of Oceangraphy, Texas A & M University. 1

Sutton, R.T. & Allen, M.R. (1997). Decadal predictability of North Atlantic sea surface temperature and climate. *Nature*, **388**, 563–567. 4, 21, 26

Valcke, S. (2013). The OASIS3 coupler: A European climate modelling community software. *Geosci. Model Dev.*, **6**, 373–388. 6

Visbeck, M., Cullen, H., Krahmann, G. & Naik, N. (1998). An ocean model's response to North Atlantic Oscillation-like wind forcing. *Geophys. Res. Lett.*, **25**, 4521–4524. 3, 15

von Storch, H. & Zwiers, F.W. (1999). *Statistical Analysis in Climate Research*. Cambridge University Press. 8, 10, 11, 12

Weaver, A.J., Sedláček, J., Eby, M., Alexander, K., Crespin, E., Fichefet, T., Philippon-Berthier, G., Joos, F., Kawamiya, M., Matsumoto, K., Steinacher, M., Tachiiri, K., Tokos, K., Yoshimori, M. & Zickfeld, K. (2012). Stability of the Atlantic meridional overturning circulation: A model intercomparison. *Geophy. Res. Lett.*, **39**. 31

Wilks, D.S. (1995). *Statistical Methods in the Atmospheric Sciences*. Academic Press. 8

Wunsch, C. (2002). What is the thermohaline circulation? *Science*, **298**, 1180–1181. 1

Statement / Erklärung

I hereby declare that I have written the bachelors thesis on my own and have used no other than the stated sources and aids. The submitted written version is equivalent to the electronical data medium. Furthermore, I affirm that this work has not been submitted for any other degree.

Hiermit erkläre ich, dass ich die vorliegende Bachelorarbeit selbstständig und ohne fremde Hilfe angefertigt und keine anderen als die angegebenen Quellen und Hilfsmittel verwendet habe. Die eingereichte schriftliche Fassung der Arbeit entspricht der auf dem elektronischen Speichermedium. Weiterhin versichere ich, dass diese Arbeit noch nicht als Abschlussarbeit an anderer Stelle vorgelegen hat.

Kiel, July 23, 2013 Milan Klöwer